Endosome mediated delivery of ceramide phosphoethanolamine (CPE) with unique acyl chain anchors to the cleavage furrow is essential for male meiosis cytokinesis.

Govind Kunduri[1*], Si-Hung Le [2], Nagampalli Vijayakrishna[3], Daniel Blankenberg[3], Yoshihiro, Izumi[2], Takeshi Bamba[2], Usha Acharya[1*] and Jairaj K.Acharya[1]*.

1. Cancer and Developmental Biology Laboratory, National Cancer Institute, Frederick, MD 21702.
2. Department of Metabolomics, Kyushu University, Fukuoka 812-8582, Japan.
3. Genomic Medicine Institute and Lerner Research Institute, Cleveland Clinic, Cleveland, OH.

* Corresponding authors: kunduri.govind@nih.gov; usha.acharya@nih.gov ; acharyaj@mail.nih.gov

Abstract

Division of one cell into two daughter cells is fundamental in all living organisms. Cytokinesis, the final step of cell division, begins with the formation of an actomyosin contractile ring, positioned midway between the segregated chromosomes. Constriction of the ring with concomitant membrane deposition in a spatiotemporal precision generates a cleavage furrow that physically divides the cytoplasm. Unique lipids with specific biophysical properties have been shown to localize to midbodies however, their delivery mechanisms and biological roles were largely unknown. In this study, we show that Ceramide phosphoethanolamine (CPE), the structural analog of sphingomyelin, has unique acyl chain anchors in spermatocytes and is essential for meiosis cytokinesis. We found that disengagement of the central spindle from the contractile ring but not localization of phosphatidyl inositols (PIPs) at the plasma membrane was responsible for the male meiosis cytokinesis defect in CPE deficient animals. Further, we demonstrate that enrichment of CPE in Rab7 and Rab11 positive endosomes which in turn translocate to the cleavage furrows to promote cytokinesis. Our results implicate endosomal delivery of CPE to ingressing membranes is crucial for meiotic cytokinesis.

Introduction

Eukaryotic cells display high diversity in lipid species, that are chemically and structurally distinct. They are classified into eight major categories, each of which is further subdivided into classes and subclasses [1]. Lipids usually comprise of a polar head group that is linked by a structural backbone to hydrophobic tail groups composed of acyl chains. Lipid diversity that exists in cells arises from the large number of combinatorial chemical possibilities that the head and tail moieties could generate. Diversification of lipids to cope with evolving cellular complexity has resulted in thousands of lipid species each with purported unique function most of which still remain unknown [2].

The head group of each lipid class has been widely recognized for its biological function. For instance, the inositol head group of phosphatidylinositols and its modifications play critical roles in cellular signaling [3]. However, even within each lipid class, there are a number of molecularly distinct species that have identical head group but differ extensively in their acyl side chains such as number of carbon atoms, number of double bonds and the nature of the chemical linkage (e.g., ester or ether). An increasing number of studies are beginning to reveal the importance of acyl side chains by demonstrating that they selectively bind to target proteins and elicit biological function [4, 5]. For instance, a recent study has shown that acyl side chains of diacylglycerol significantly influence the recruitment of protein kinase C to the plasma membrane [6]. Similarly, Ceramide chain length was shown to be critical for selective protein cargo sorting at endoplasmic reticulum (ER) exit sites in yeast [7]. The COPI machinery protein p24 was shown to bind specifically to N-stearoyl sphingomyelin (SM C18) and acts as a cofactor to regulate COPI-dependent transport in the early secretory pathway. Further, this interaction depended on both the headgroup and the backbone of the sphingolipid [8].

57 Cell division is fundamental to all living organisms where one cell divides into two daughter cells.
58 The last step of cell division, the cytokinesis, begins with the formation of an actomyosin
59 contractile ring, positioned midway between the segregated chromosomes. Narrowing of this ring
60 with the addition of membrane in a spatiotemporally defined mode produces a cleavage furrow
61 that physically divides the cytosol [9]. During somatic cytokinesis, the two daughter cells are
62 interconnected *via* midbodies prior to abscission. Although these structures are transient, they
63 accumulate defined lipid species to mediate correct cell division [10-12]. Unlike somatic
64 cytokinesis, in testis, the developing spermatogonial cells divide synchronously with an
65 incomplete cytokinesis where all the daughter cells remain interconnected by cytoplasmic bridges.
66 Thus, the spermatogonial cells develop as a syncytium and become separated from each other only
67 at the end of spermatogenesis during spermatid individualization. The high degree of membrane
68 curvature necessary for cleavage furrow constriction and stabilization of intercellular bridges
69 (ICB)/cytoplasmic bridges necessitates lipid components with specific biophysical properties.
70 While the presence of very long chain fatty acids (which are components of sphingolipids and
71 glycosphingolipids) in cytokinesis has been shown, the relationship between membrane lipid
72 composition, ring constriction and furrow ingression is still underexplored. Although
73 sphingomyelins containing very long chain plyunsaturated fatty acids (VLC-PUFAs) were
74 identified in various mammalian testis including humans, their direct role in spermatogenesis
75 particularly in meiosis cytokinesis remains unknown [13, 14].
76 In this study we show that CPE, the structural analog of sphingomyelin (SM), has unique acyl
77 chain anchors in spermatocytes and CPE is essential for meiosis cytokinesis, spermatid polarity
78 and individualization. The head group of CPE is also important for spermatogenesis. Ceramide
79 phosphoethanolamine synthase (CPES) expression in transit amplifying to spermatocyte stage is

80 essential for successful completion of spermatogenesis. We show aberrant central spindle behavior
81 at the cleavage furrows is responsible for the meiosis cytokinesis defect. Further, we show
82 endocytically retrieved CPE from plasma membrane is enriched in Rab7 containing endosomes
83 and targeted to cleavage furrows during cytokinesis demonstrating the importance of CPE rich
84 membrane addition at the cleavage furrows.

85 ## Results

86 **Sphingosine with VLC-mono-unsaturated fatty acid and sphingadiene with VLC-saturated**
87 **fatty acid containing sphingolipids are enriched in the testis**

88 To investigate sphingolipid species diversity and their role in *Drosophila* tissues we performed
89 super-critical fluid chromatography coupled to mass spectrometry (SFC/MS/MS) on extracted
90 lipids from wild type fly head, dissected ovary and testis (Data S1). As shown in Fig.1A. CPE is a
91 more abundant sphingolipid compared to ceramides (Fig.1B) and hexosylceramides (HexCer)
92 (Fig.1C). The amount of CPE is significantly higher in testis compared to head and ovary (Fig.1A).
93 In contrast hexosylceramides were significantly higher in the heads compared to ovary and testis
94 (Fig.C).

95 ***Fig.1. Sphingolipid analysis in wild type Drosophila tissues.*** *(A-C) Sphingolipids were extracted*
96 *from wild type male and female heads and dissected ovary and testes using Methanol:Chloroform*
97 *method and subjected to SFC/MS/MS. Wild type heads from male flies (WTHM), wild type heads*
98 *from female (WTHF), wild type ovary (WTOY) and wild type testis (WTTS). Sphingolipids were*
99 *quantitated by measuring large fragments in MRM and average amounts from 3 independent*
100 *biological replicates were shown as picomols (pmol) in 100 micrograms of carbon. Each*
101 *sphingolipid species (CPE (1A), Ceramide (1B) & HexCer (1C)) was further subdivided into 5*
102 *major subspecies. Each of the subspecies differed in acyl chain length but contained similar*

103 *chemical properties Dihydrosphingosine (DHSPH) base linked to Saturated fatty acid (SFA)*
104 *(DHSPH_SFA), Sphingosine (SPH) base linked to SFA (SPH_SFA), Sphingosine (SPH) base*
105 *linked to Monounsaturated fatty acid (MUFA) (SPH_MUFA), Sphingosine (SPH) base linked to*
106 *Polyunsaturated fatty acid (2-6 double bonds, PUFA) (SPH_PUFA) and Sphingadiene (SPD)*
107 *with SFA (SPD_SFA). (D) Cartoon showing the chemical structure of three major CPE subspecies*
108 *including CPE_SPH_SFA, CPE_SPH_MUFA and CPE-SPD_SFA. (E) CPE subspecies within*
109 *CPE_SPH_SFA that differed in number of carbon atoms in acyl chains of sphingosine base and*
110 *fatty acid. (F) CPE subspecies within CPE_SPH_MUFA. (G) CPE subspecies within*
111 *CPE_SPD_SFA. Statistical significance was calculated using mean, standard deviation (SD) and*
112 *N in Prism 8. The 2way ANOVA multiple comparisons was used to calculate P values where ****P*
113 *≤ 0.0001;***P ≤ 0.001; **P ≤ 0.01; *P ≤ 0.05 and ns P >0.05. Three independent biological*
114 *replicates were performed for each sample and lipids were extracted from 400 heads or 250 pairs*
115 *of ovary or testis for each biological replicate.*
116 Closer examination of acyl chain composition revealed that head and ovary derived CPEs are
117 predominantly composed of sphingosine linked to saturated fatty acid (SPH-SFA) (Fig.1D and
118 1E). Interestingly, in addition to SPH-SFA, CPE in the testis is enriched in two distinct species
119 with net two double bonds in their acyl chain composition including sphingosine (one double
120 bond) linked to mono-unsaturated fatty acid (SPH- MUFA) (Fig.1D and 1F) and a sphingadiene
121 (two double bonds) linked to saturated fatty acid (SPD-SFA) (Fig.1D and 1G). The fatty acid acyl
122 chain lengths of these CPE species are predominantly composed of C20, C22, C24 and therefore
123 could be classified as very long chain (VLC) sphingolipids. The sphingoid base acyl chain length
124 composed of d14 and d16 (Fig.1F and 1G). The corresponding ceramide precursors are also
125 evident in the wild type testis samples indicating acyl chain diversity is likely introduced during

126 ceramide synthesis but not after CPE synthesis (Fig.1B and Data S1). Remarkably, SPH_MUFA
127 and SPD_SFA were also present in HexCer but at significantly lower levels in the testis compared
128 to heads (Fig.1C vs Fig.1A). The fatty acid acyl chain length of HexCer SPH_MUFA and
129 HexCer_SPD_SFA showed that they are predominantly composed of C18 and C20 while the
130 sphingoid base is composed of primarily d14 and d16 (Fig.S1B and S1D). HexCer with d14
131 sphingosine base and C22 PUFA (SPH-PUFA) is enriched in heads compared to testis (Fig.1C and
132 Fig.S1C). Taken together these results suggest that CPE in the testis and the HexCer in the central
133 nervous system have unique acyl chain composition.

134 ***Fig.S1. Comparison of hexosylceramides and its subspecies in Drosophila tissues.*** *(A)*
135 *Hexosylceramides composed of sphingosine base linked to saturated fatty acid (HexCer SPH-SFA)*
136 *and its subspecies were shown as picomols (pmol) in 100 micrograms of carbon. Wild type heads*
137 *from male flies (WTHM), wild type heads from female (WTHF), wild type ovary (WTOY) and wild*
138 *type testis (WTTS). (B) Hexosylceramides and its subspecies composed of sphingosine base linked*
139 *to Monounsaturated fatty acid (HexCer-SPH-MUFA). (C) Hexosylceramides and its subspecies*
140 *composed of sphingosine base linked to Polyunsaturated fatty acid (HexCer-SPH-PUFA). (D)*
141 *Hexosylceramides and its subspecies composed of Sphingadiene base linked to Saturated fatty*
142 *acid (HexCer SPD-SFA). Statistical significance was calculated using mean, standard deviation*
143 *(SD) and N in Prism 8. The 2way ANOVA multiple comparisons was used to calculate P values*
144 *where ****$P \leq 0.0001$;***$P \leq 0.001$; **$P \leq 0.01$; *$P \leq 0.05$ and ns $P > 0.05$. Three independent*
145 *biological replicates were taken for each sample and lipids were extracted from 400 heads or 250*
146 *pairs of ovary or testis for each biological replicate.*

147 **CPE deficient males are sterile and show defects in male meiotic cytokinesis, spermatid**
148 **polarity and individualization**

149 To understand the biological significance of the unique CPE species in the testis, we reasoned that
150 the *cpes* null mutant generated by us would serve as a suitable tool since *cpes* mutant males are
151 sterile [15]. These mutants show accumulation of germ cells at the tip of the testis and absence of
152 mature sperms in seminal vesicles (Fig.2B). To investigate cytological defects in *cpes* mutant
153 testis, we have performed live testis squash preparation followed by phase contrast microscopy.
154 This method allows for easy identification of almost all of the major stages of spermatogenesis
155 [16]. During meiotic divisions, chromosomes and mitochondria are equally partitioned to each of
156 the four daughter cells. Immediately following meiosis, in the round spermatid stage, mitochondria
157 in each daughter cell aggregate to form a large phase dark structure known as the nebenkern.
158 Round spermatids (onion stage spermatids) are characterized by phase dark nebenkern and phase
159 light nucleus at roughly equal size and at a ratio of 1:1 per daughter cell. The nuclear size of round
160 spermatid is directly proportional to the chromatin content, hence any errors in chromosome
161 segregation during meiosis can lead to variability in nuclear size [17, 18]. Similarly defects in
162 meiotic cytokinesis following normal chromosome segregation results in cells with two or four
163 nuclei and an abnormally large nebernkern. These changes can be easily visualized by phase
164 contrast microscopy and is often used as a diagnostic to detect male meiotic defects [18-24]. As
165 shown in Fig.2D, wild type round spermatids contained an equal sized phase light nucleus and a
166 phase dark nebenkern at a ratio of 1:1 per cell within the cyst of 64 cells. In contrast *cpes* mutant
167 round spermatids showed four regularly sized nuclei (tetranucleate) and one abnormally large
168 nebenkern, indicating a failure in cytokinesis in both meiosis I and II divisions (Fig.2E).

169 ***Fig.2. Cytological, immunofluorescence and sphingolipid analysis in cpes mutants.***

170 *(a-c) whole mount of Drosophila testis immunostained for germ cell specific Vasa protein primary*
171 *antibody and Alexa fluor 488 secondary antibody to visualize various stages of germ cells*

172 *including stem cells, spermatogonia and spermatocytes (A) w^{1118}, (B) cpes mutant and (C) Tub-*
173 *Gal4>UAS CPES rescue. (D-F) Phase contrast microscopy of live testis squash preparations to*
174 *visualize round/onion stage spermatids (D) w^{1118}, (E) cpes mutant and (F) Tub-Gal4>UAS CPES*
175 *rescue. (G-I) Testis squash preparation followed by fixation and immunostaining to visualize early*
176 *elongating spermatids. The beta tubulin primary antibody and Alexa fluor 568 conjugated*
177 *secondary antibody were used for immunostaining, w^{1118} (G), cpes mutant (H) and Tub-Gal4>UAS*
178 *CPES rescue (I). (J-K) whole mount Drosophila testis immunostained with cleaved caspase*
179 *specific DCP-1 primary antibody and Alexa fluor 568 secondary antibody to visualize*
180 *individualizing spermatids (J) w^{1118} (K) cpes mutant and (L) Tub-Gal4>UAS CPES rescue. (M-O)*
181 *Sphingolipid analysis in lipid extracts of dissected testis. (M) Comparison of CPE and its*
182 *subspecies between w^{1118}, cpes mutant and bam-Gal4>UAS CPES rescue. (N) Comparison of*
183 *ceramide and its subspecies between w^{1118}, cpes mutant and bam-Gal4>UAS CPES rescue. (O)*
184 *Comparison of hexosylceramide and its subspecies between w^{1118}, cpes mutant and bam-*
185 *Gal4>UAS CPES rescue. Statistical significance was calculated using mean, standard deviation*
186 *(SD) and N in Prism 8. The 2way ANOVA multiple comparisons was used to calculate P values*
187 *where ****$P \leq 0.0001$;***$P \leq 0.001$; **$P \leq 0.01$; *$P \leq 0.05$ and ns $P > 0.05$. Three independent*
188 *biological replicates were taken for each sample and 250 pairs of testis were used for lipid*
189 *extraction from each biological replicate.*

190 Following the round/onion stage, the 64 interconnected haploid cells in the cyst become highly
191 polarized with the nucleus localizing to one end and the sperm tail (axoneme) growing in the
192 opposite side. These elongating spermatid nuclei face towards the seminal vesicles and the tails
193 grow towards the germline stem cell hub/tip of the testis. As shown in Fig.2G, wild type early
194 elongating spermatids had all the nuclei facing one side and their axoneme growing to the opposite

195 side indicating that they are highly polarized. In contrast, elongating spermatids in *cpes* mutant
196 cysts appeared as sickle cell shaped with the nuclei present in the middle-bulged area (ocassionally
197 throughout the cyst) and their tails growing on both sides of the cyst (Fig.2H). This data indicates
198 that spermatid polarity is compromised in *cpes* mutants.
199 Individualization is the final stage of spermatid differentiation wherein structures called
200 individualization complex (IC) containing actin cones assemble at the head/rostral end of
201 elongated spermatids and start moving away from the nuclei towards the tail/caudal end of the
202 cyst. As the IC travels it removes the cytoplasmic contents of the cyst and will individualize each
203 spermatozoon with its own plasma membrane. The extruded cytoplasmic contents are collected
204 into a sac like structure called the 'cystic bulge' that forms around the IC. As this process proceeds
205 and the IC and cystic bulge reach the end of the flagella, the actin cones and cytoplasmic contents
206 are extruded in a waste bag, the contents of which are degraded later [25]. Activated caspases
207 have a non-apoptotic role in cystic bulge and the waste bag of individualizing spermatids and are
208 essential for successful spermatid individualization [26]. Immunostaining of wild type testis with
209 *Drosophila* Caspase 1 (DCP-1) antibody showed elongated spermatids undergoing
210 individualization that contained cystic bulges and waste bags (Fig.2J). In contrast, *cpes* mutant
211 testis showed defectively elongated spermatids and were devoid of cystic bulges and waste bags
212 indicating failure in spermatid individualization (Fig.2K).
213 Ubiquitous expression of wild type cDNA copy of CPES completely rescued male sterility. As
214 shown in Figs.2C, f, i and l, phase contrast imaging of live testis squash preparations showed 1:1
215 nebenkern to nucleus ratio indicating rescue of meiotic cytokinesis defect (Fig.2F). Further
216 immunostaining of testis squash preparations with tubulin antibody and DAPI showed that
217 spermatid polarity was completely restored wherein all the nuclei face one side and their tails face

218 the other side of the cyst (Fig.2I). DCP-1 staining showed individuating spermatids with cystic
219 bulges and waste bags indicating normal individualization (Fig.2L).
220 To investigate the sphingolipid content in *cpes* mutant we dissected wild type, *cpes* mutant and
221 germ cell specific rescue (Bam Gal4> UAS CPES) testes were dissected, sphingolipids were
222 extracted and analyzed by SFC/MS/MS as described in the methods (Data S1). There was complete
223 loss of CPE in *cpes* mutant testis (Fig.2M) and expression of CPES only in the germs cells was
224 sufficient to restore CPE to near wild type level. The mutant and rescue samples were processed
225 at the same time as the wild type for mass spectrometry, hence the wild type testis sample is the
226 same as in Fig.1 (Data S1). Loss of CPE synthesis in *cpes* mutants caused concurrent accumulation
227 of ceramides particularly SPH-MUFA and SPD-SFA species (Fig.2N) and expression of CPES in
228 germ cells reduced ceramide levels. HexCer levels were also slightly increased in *cpes* mutant
229 testis (Fig.2O), interestingly expression of CPES in germ cells did not reduce the HexCer levels
230 indicating their levels did not correlate with the *cpes* mutant phenotypes in the testis.

231 **CPES enzymatic activity is required for spermatogenesis and accumulation of ceramide is**
232 **not the cause for spermatogenesis defects**

233 In order to determine whether enzymatic activity of CPES is required for spermatogenesis we have
234 generated active site mutants of CPES. The CPES has conserved amino acid motif D(X)2DG(X)2
235 (A/Y)R(X)8-16G(X)3D(X)3D in the CDP-alcohol phosphotransferase domain (CAPT) [27]. The
236 final aspartates of this motif were shown to be essential for catalysis of human
237 choline/ethanolamine phosphotransferase CEPT1 [28, 29]. We substituted the last two active site
238 aspartates of CPES with alanine residues and subcloned into pUAST vector for generating
239 transgenic flies. The UAS_CPES (DX_3D to AX_3A) mutant transgene was expressed in *cpes* mutant
240 background using Bam Gal4 to test rescue of spermatogenesis phenotypes. As shown in Fig.S2A

241 and B, the active site mutant did not rescue spermatogenesis phenotypes suggesting a crucial role
242 for CPES enzymatic activity in spermatogenesis.

243 ***Fig.S2. CPES enzymatic activity is required for spermatogenesis and accumulation of ceramide***
244 ***is not responsible for cpes mutant phenotypes.*** *(A-C) Live testis squash preparation followed by*
245 *phase contrast microscopy of round spermatids (A) The UAS CPES active site mutant (GX_3DX_3D*
246 *to GX_3AX_3A) was expressed using Bam-Gal4 in cpes mutant background. (B) cpes; dcert double*
247 *mutants (C) The UAS CDase (neutral ceramidase) was expressed using Bam-Gal4 driver in cpes*
248 *mutant background.*

249 We next investigated whether accumulation of ceramide at the Golgi is responsible for the
250 observed phenotypes. Ceramide is generated in the membranes of endoplasmic reticulum (ER) via
251 the *de novo* biosynthetic pathway catalyzed by the rate limiting enzyme serine palmitoyltransferase
252 (SPT). Subsequently ceramide is actively transported from ER to Golgi via ceramide transfer
253 protein (DCERT) and thus absence of DCERT could prevent ceramide accumulation at the Golgi
254 [30]. To investigate whether blocking ceramide transport from ER to Golgi could restore
255 spermatogenesis, we have generated *cpes* and $dcert^1$ double mutants and their testis was analyzed
256 for meiotic cytokinesis and spermatid polarity phenotypes. However, as shown in Fig.S2C and D.
257 *cpes*; $dcert^1$ double mutants did not rescue meiotic cytokinesis and spermatid polarity indicating
258 ceramide accumulation may not be responsible for the phenotypes. In *Drosophila*, transgenic
259 expression of neutral ceramidase was shown to reduces ceramide levels *in vivo* [31]. To further
260 confirm, we have overexpressed ceramidase (UAS CDase) in germs cells using Bam-Gal4 in *cpes*
261 mutant background and the progeny testis was analyzed for the rescue of mutant phenotypes.
262 However, again expression of CDase did not rescue meiosis cytokinesis and spermatid polarity
263 (Fig.S2E and F) suggesting that absence of CPE but not accumulation of ceramide is responsible

264 for the phenotypes. Also, ceramide levels in testis do not correlate with sterility as will be discussed
265 in figure 4J and K.

266 **Genetic dissection of spatiotemporal role of CPES in spermatogenesis**

267 To determine the stage of germ cell differentiation at which CPES expression has an important
268 role, we have performed cell type/stage specific rescue experiments using UAS/Gal4 system in the
269 *cpes* mutant background (Fig.3A). We first expressed UAS CPES in cyst cells using C587-Gal4
270 to investigate a possible non-cell autonomous role. However, as shown in Fig.3, expression of wild
271 type CPES in cyst cells did not rescue meiotic cytokinesis, spermatid polarity and individualization
272 (Fig.3 B, F and J respectively). We next expressed wild type UAS CPES in germ cells using three
273 different Gal4 drivers that have been previously shown to be specifically expressed in stem cells
274 (nos-Gal4), transit amplifying spermatogonial cells (bam-Gal4) and late spermatocytes (chif-Gal4)
275 (Fig.3A). Interestingly, we observed varying degree of rescue, depending on the germ cell
276 differentiation stage at which UAS CPES was expressed. The nos-Gal4 dependent expression of
277 UAS CPES partially rescued both meiosis cytokinesis and spermatid polarity (Fig.3C, and G)
278 however, individualizing spermatids lacked cystic bulges and waste bags indicating
279 individualization was not fully rescued (Fig.3K). The bam-Gal4 dependent expression of UAS
280 CPES in transit-amplifying cells completely rescued meiosis cytokinesis, spermatid polarity and
281 individualizing spermatids contained cystic bulges and waste bags (Fig.3D, H and L). In contrast,
282 only partial rescue of meiosis cytokinesis was observed when UAS CPES was expressed in
283 spermatocytes using chif-Gal4 (Fig.3E). Although, the spermatid polarity was completely rescued,
284 the individualizing spermatids largely lacked cystic bulges and waste bags indicating that
285 individualization was defective (Fig.3I and M).

286 ***Fig.3. Genetic dissection of spatiotemporal role of CPES in spermatogenesis.*** *(A) Schematic*
287 *illustration of early germ cell differentiation and the stage specific Gal4 expression patterns. The*
288 *C587-Gal4 expresses in somatic cyst cells, nos-Gal4-VP16 expresses in GSCs and spermatogonia,*
289 *bam-Gal4-VP16 expresses in 4-16 stages of spermatogonia to spermatocytes, and Chif-Gal4*
290 *expresses in early spermatocytes. (B-E) Phase contrast microscopy of round spermatids in live*
291 *testis squash preparations. (F-I) Early elongating spermatids immunostained for beta tubulin*
292 *primary antibody (Alexa 568) and DAPI for DNA (J-M) Individualizing spermatids*
293 *immunostained for cleaved caspase DCP-1 antibody and DAPI for DNA. (B,F and J) C587-Gal4*
294 *drives the expression of UAS CPES in cyst cells of cpes mutants. (C, G and K) Nanos-Gal4 drives*
295 *the expression of UAS CPES in GSCs and spermatogonia. (D, H & I) bam-Gal4 drives the*
296 *expression of UAS CPES in spermatogonia and spermatocytes (E, I & M) chif-Gal4 drives the*
297 *expression of UAS CPES in early spermatocytes. (N) Male fertility test where individual males*
298 *from each of the UAS CPES rescue experiment was crossed with 3 wild type females. The vials*
299 *which produced at least 5 pupae or progeny were counted as fertile and plotted as percent fertility*
300 *compared to wild type males. (O-R) Whole mount immunostaining followed by confocal imaging*
301 *of genomic CPES flies where CPES is tagged with V5 at the C-terminus (red). The GM130 was a*
302 *cis-Golgi marker (green) and DAPI (blue) stains the DNA.*

303 To determine the extent to which male fertility was rescued by cell type specific CPES expression
304 compared to wild type, we performed the male fertility test as described in the methods section.
305 As shown in Fig.3N, expression of UAS CPE in transit amplifying spermatogonial cells and
306 spermatocytes (bam-Gal4) rescued male fertility to wild type levels. In contrast only partial rescue
307 was observed when UAS CPES was expressed only in stem cells (nos-Gal4) or in spermatocytes

308 (chif-Gal4). Expression of UAS CPES in cyst cells (C587-Gal4) did not rescue male sterility and
309 as all of the males were sterile (Fig.3N).
310 To determine *in vivo* CPES expression more precisely at the protein level, we have expressed
311 genomic CPES tagged with V5 at the C-terminus. Immunostaining followed by confocal imaging
312 showed that CPES_V5 was highly expressed in the cells that are present just below the tip of the
313 testis (Fig.3O and R). This area of the testis is known to be enriched in spermatogonia and early
314 spermatocytes [16].
315 Taken together these results show that testis specific CPE generation by CPES from transit
316 amplification stage to spermatocyte stage is crucial for successful meiosis cytokinesis, spermatid
317 polarity and spermatid individualization.
318 **Insect CPE Synthases but not sphingomyelin Synthase rescue male sterility defects**
319 Previously we have shown that CPE has an important structural role in cortex glial plasma
320 membranes [15]. The cortex glial plasma membranes are severely defective in *cpes* mutants
321 leading to loss of cortex glia neuronal cell body interactions during development and increased
322 susceptibility to light inducible epilepsy in adults. Further, we have shown that overexpression of
323 human sphingomyelin synthase 1 (hSMS1) that produces SM instead of CPE was sufficient to
324 rescue cortex glia plasma membrane defects via establishment of detergent resistant membranes.
325 We wondered whether overexpression of hSMS1 could also rescue the spermatogenesis
326 phenotypes of *cpes* mutant. To this end, UAS hSMS1 was overexpressed using Tubulin-Gal4 in
327 *cpes*, the adult male testes were dissected, and live testis squash preparations were observed using
328 phase contrast microscopy. However, as shown in Fig.4A, hSMS1 overexpression did not rescue
329 male meiosis cytokinesis. Further, immunostaining analysis showed that spermatid polarity was
330 also not rescued (Fig.4E) suggesting an important role for the CPE head group in spermatogenesis.

331 We next investigated whether overexpression of other insect derived CPES could rescue *cpes*
332 mutant phenotypes. To test this, we have overexpressed *Aedes aegypti* (Yellow fever mosquito,
333 60% identity and 77% similarity), *Bombyx mori* (domestic silk moth, 43% identity and 58%
334 similarity) and *Tetranychus urticae* (two-spotted spider mite, 33% identity and 51% similarity)
335 derived UAS CPES homologs in *cpes* mutant background using Tubulin-Gal4. As shown in Fig.4
336 mosquito and silk moth CPES were able to completely rescue meiosis cytokinesis (Fig.4B and C)
337 and spermatid polarity (Fig.4F and G). However, spider mite CPES was not able to rescue any of
338 the *cpes* phenotypes (Fig.4D and H).

339 ***Fig.4. Insect CPE synthases but not sphingomyelin synthases rescue spermatogenesis defects.***
340 *(A-D) Phase contrast microscopy of round spermatids where UAS hSMS1 (A), UAS Aedes CPES*
341 *(B), UAS Bombyx CPES (C), and UAS T.Urticae CPES (D) were ubiquitously expressed in cpes*
342 *mutant background using Tubulin Gal4. The scale bar is equivalent to 10 μm. (E-H) Confocal*
343 *images of elongating spermatids immunostained with beta tubulin primary antibody and Alexa*
344 *fluor 568 secondary antibody and DAPI for DNA. The UAS hSMS1 (E), UAS Aedes CPES (F),*
345 *UAS Bombyx CPES (G), and UAS T.Urticae CPES (H). (I-L) Sphingolipid analysis of lipids*
346 *extracted from testis of wild type, cpes mutant, and various rescues expressed in germ cells using*
347 *Vasa-Gal4. In contrast to Figs.1 and 2, here we used whole male organ (testis, accessory glands,*
348 *collecting ducts and ejaculatory bulb) for lipid extraction. (I) The amounts of CPE and its*
349 *subspecies in wild type, cpes mutant and various rescues were shown. (J) Ceramide and its*
350 *subspecies were shown in picomoles per 100μg of carbon. (K) Hexosylceramides and its major*
351 *subspecies amounts were shown in bar diagram. (L) Amount of sphingomyelin and its subspecies*
352 *were shown as picomoles per 100μg of carbon. Dihydrosphingosine (DHSPH), Sphingosine*
353 *(SPH), Sphingadiene (SPD) Saturated fatty acid (SFA), Monounsaturated fatty acid (MUFA) and*

354 *polyunsaturated fatty acid (PUFA). Statistical significance was calculated using mean, standard*
355 *deviation (SD) and N in Prism 8. The 2way ANOVA multiple comparisons was used to calculate*
356 *P values where ****P ≤ 0.0001;***P ≤ 0.001; **P ≤ 0.01; *P ≤ 0.05 and ns P >0.05. Three*
357 *independent biological replicates were taken for each sample and lipids were extracted from 250*
358 *male organs for each biological replicate.*
359 To investigate the nature of sphingolipid species synthesized by hSMS1, *Aedes aegypti*, *Bombyx*
360 *mori* and *Tetranychus urticae* derived CPES, we have specifically expressed these transgenes in
361 germ cells using vasa-Gal4, their male reproductive system was dissected, lipids were extracted
362 and subjected to sphingolipid analysis using SFC/MS/MS as described in the methods section
363 (Data S2). As shown in Fig.4I germ cell specific expression of *Drosophila* CPES, *Bombyx mori*
364 CPES completely restored CPE to the wild type amounts. *Aedes aegypti* CPES also synthesized
365 significant amount of CPE but to a lower amount than *Drosophila* CPES. However, all three
366 distinct CPE species are synthesized by *Aedes aegypti* CPES and *Bombyx* CPES (Fig.4I). As
367 anticipated, hSMS1 did not synthesize CPE (Fig4I but produced significant amount of SM
368 (Fig.4L). However, the amount of SM is relatively low compared to CPE, perhaps due to limited
369 expression/stability of hSMS1 in germ cells (vasa-Gal4). Indeed, ubiquitous expression of hSMS1
370 using actin-Gal4 driver significantly increases the SM amounts (Fig.4M), yet at this level of
371 expression we did not see rescue of *cpes* mutant phenotypes (Fig.4A and E) suggesting the
372 importance of the CPE head group. We next analyzed the ceramide content in these samples and
373 found that ceramide levels were significantly high in *cpes* mutants and hSMS1 rescue compared
374 to *Drosophila* CPES rescue. Interestingly, even though *Tetranychus urticae* CPES was not able to
375 synthesize CPE, it significantly reduced the ceramide and HexCer amounts of *cpes* mutants (Fig.4
376 J, and K). However, despite the reduction in ceramide and HexCer levels, *Tetranychus urticae*

377 CPES failed to rescue *cpes* mutant phenotypes suggesting lack of correlation between ceramide
378 accumulation and rescue of *cpes* mutant phenotypes (Fig.4J). Similarly, higher amounts of HexCer
379 in *Aedes aegypti* CPES rescue and *Bombyx mori* CPES rescue did not correlate with the
380 spermatogenesis phenotype rescue (Fig.4K).

381 **Aberrant central spindle behavior but not localization of PIPs at the plasma membrane is**
382 **responsible for defective meiosis cytokinesis in *cpes* mutants**

383 To determine the mechanism by which CPES regulates meiosis cytokinesis we have performed
384 RNAseq with total RNA isolated from dissected testis from w^{1118}, *cpes* mutant and bam-
385 Gal4>UAS CPES rescue. Gene set enrichment analysis (GSEA) comparison between w^{1118} (WT),
386 *cpes* (KO) and rescue (RES) samples indicated that several pathways involved in spindle
387 organization, metabolism, endocytosis, signaling, male meiosis cytokinesis, spermatid
388 differentiation, sperm individualization etc., are significantly altered in *cpes* mutants (Fig.5A). Red
389 bars in the Fig.5A indicates gene sets enriched in *cpes* mutants and blue bars indicate gene sets
390 enriched WT & RES. GSEA showed several genes involved in spindle organization and spindle
391 elongation positively correlated with the mutant phenotype (Fig.5B and C). The heat map
392 comparison for genes involved in spindle organization and elongation are shown in Data S3 and
393 S4. To study spindle behavior during male meiosis cytokinesis *in vivo*, we performed live imaging
394 on isolated cysts. We first dissected the testis in M3 insect cell culture media and muscle sheath
395 was cut open to release intact spermatocyte cysts into the media. Subsequently spermatocyte cysts
396 were transferred to poly-D-lysine coated cover glass dishes and live imaging was performed using
397 Andor spinning disk confocal microscopy as described in the methods section. We chose mCherry
398 tagged microtubule cross linking protein Feo (Ubi-p63E-feo-mCherry) as a marker for central
399 spindle. Feo-mCherry was shown to accumulate at the anaphase B and telophase central spindle

400 [32]. We have also used spaghetti squash (sqh) gene encoding myosin II regulatory light chain
401 (RLC) tagged to GFP (Sqh-GFP-RLC) as a marker for actin-myosin based structure known as
402 contractile ring that assembles during late anaphase [33]. The actin and myosin ring positioned
403 midway between two spindle poles is thought to drive the formation of the cleavage furrow during
404 telophase. As shown in Movie S1, Fig.5D, the actomyosin ring (Sqh-GFP-RLC) quickly assembles
405 around the central spindle during late anaphase and both simultaneously constrict through early to
406 late telophase. At the end of late telophase Feo-mCherry disassembles however, Sqh-GFP-RLC
407 remains and becomes part of ring cannal/cytoplasmic bridges between daughter cells (Movie S1).
408 Interestingly, in *cpes* mutants, the initial assembly of central spindle and actomyosin ring occurred
409 normally (Movie S2) however, central spindle and actomyosin ring constriction became uneven
410 during cleavage furrow ingression leading to substantial disengagement between them (Fig.5D).
411 As a result, central spindle disassembled prematurely leading to the cleavage furrow regression
412 and disassembly of actomyosin ring (Movie S2). Expression of UAS CPE in germ cells was
413 sufficient to rescue this phenotype (Movie S3, Fig.5D).

414 ***Fig.5. Aberrant central spindle behavior but not PIPs localization at the plasma membrane is***
415 ***responsible for meiosis cytokinesis defect in cpes mutants.*** *(A) GSEA pathway analysis of RNA*
416 *seq data from* w^{1118}*, cpes mutant and bam-Gal4>UAS CPES rescue testis. Three independent*
417 *biological replicates were taken for each sample and RNA was extracted from 200 pairs of testis*
418 *for each biological replicate. (B) Enrichment plot showing genes involved in spindle organization*
419 *are positively correlated in cpes mutants compared to* w^{1118} *and rescue. (C) Enrichment plot*
420 *showing genes involved in spindle elongation are positively correlated in cpes mutants compared*
421 *to* w^{1118} *and bam-Gal4>UAS CPES rescue. (D-F) Snapshots of live spermatocytes undergoing*
422 *meiosis I cytokinesis. Horizontal view(left), one slice of a z-stack was shown and cross-sectional*

423 *view across cleavage furrow, maximum intensity projection image was shown (right). Control*
424 *spermatocytes (top row), cpes mutant spermatocytes (middle row) and Tub-Gal4>UAS CPES*
425 *rescue (bottom row). (D) Spermatocytes expressing myosin II regulatory light chain tagged to*
426 *GFP under its own promoter (sqh) that localizes to contractile ring and mCherry tagged fascetto*
427 *(feo) expressing under the control of Ubi-p63E promoter that binds to central spindle*
428 *microtubules. (E) Spermatocytes expressing GFP tagged pleckstrin homology (PH) domain of*
429 *PLCD (UAS-PLCδ-PH-EGFP) under the control of Tub-Gal4 that localizes to plasma membrane*
430 *in the presence of phosphatidylinositol-4,5-bisphosphate (PIP2) and Ubi-p63E-Feo-mCherry. (F)*
431 *Spermatocytes expressing GFP tagged PH domain of Grp1 under the control of alpha Tub84B*
432 *promotor (tGPH) that localizes to plasma membrane in the presence of phosphatidylinositol-3,4,5-*
433 *triphosphate (PIP3) and Ubi-p63E-Feo-mCherry.*
434 Previous studies have shown that phosphatidyl inositols (PIPs) play critical roles in somatic and
435 meiotic cytokinesis [34]. Further, in somatic cells undergoing mitosis, sphingomyelin-rich lipid
436 domains in the outer leaflet of cleavage furrow were shown to be required for accumulation of PIP
437 (2) to the cleavage furrow which in turn is required for proper translocation of RhoA and
438 progression of cytokinesis. We wondered whether the distribution of PIPs at the plasma membrane
439 or at the cleavage furrow is altered in *cpes* mutants during meiosis. To investigate PIPs distribution
440 in *cpes* mutant membranes we used PIP2 reporter UAS PLCδ-PH-EGFP (UAS regulatory
441 sequence drives expression of EGFP tagged with Tag:PH(hPLCD1) and PIP3 reporter GFP-PH-
442 Steppke, also known as tGPH (an alphaTub84B promoter drives expression of EGFP fused to
443 Tag:PH(step) [35, 36].The PIP2 reporter PLCδ-PH-EGFP was shown to uniformly localize to
444 entire membrane including the cleavage furrow in *Drosophila* spermatocytes [37]. Indeed, we have
445 seen similar uniform distribution in both control and *cpes* mutant spermatocyte plasma membranes

446 indicating normal distribution of PIP2 (Movie S4 and S5, Fig.5E). Live imaging analysis on *cpes*
447 mutant spermatocytes expressing PLCδ-PH-EGFP revealed normal cleavage furrow initiation but
448 progression of furrow failed due to disconnect between central spindle and the furrow (Movie S5,
449 Fig.5E). Expression of wild type CPES restored this phenotype (Movie S6, Fig.5E). Of note,
450 PLCδ -PH-EGFP localization to spermatocyte plasma membrane was significantly reduced upon
451 loss of cyst cells while, this acute reduction did not prevent spermatocytes from completing
452 meiosis I cytokinesis. We next investigated the PIP3 distribution in control meiotic spermatocytes
453 using GFP-PH-Steppke (tGPH), interestingly, we found that tGPH localized to plasma membranes
454 and became significantly enriched at cleavage furrows (Movie S7, Fig.5F). Of note, even here, we
455 have observed that plasma membrane localization and cleavage furrow enrichment of tGPH
456 strictly depended on the intact cyst. While it is currently unknown if PIP3 localization to the
457 spermatocyte cleavage furrows has any impact on cytokinesis, a recent study has shown that
458 cytohesin Steppke reduces tissue tension by inhibiting the actomyosin activity at adherens
459 junctions and actomyosin network assembly is necessary and sufficient for local Steppke
460 accumulation in *Drosophila* embryos [38]. We next wondered cleavage furrow enrichment of PIP3
461 is altered in *cpes* mutants. However, as shown in Movie S8, Fig5F, PIP3 localization to the
462 cleavage furrows was not altered but again there was a disconnect between cleavage furrow and
463 central spindle during cleavage furrow ingression. Expression of wild type CPES restored this
464 phenotype (Movie S9; Fig.5F). Overall, these observations suggest that aberrant spindle behavior
465 but not the localization of PIPs to the plasma membrane or cleavage furrow, is responsible for
466 meiotic cytokinesis defect in *cpes* mutants.

467 **CPE endocytosis and targeting to cleavage furrows occurs during meiosis cytokinesis**

468 To determine how CPE is promoting the synergy between central spindle constriction and cleavage
469 furrow ingression during cytokinesis we have utilized recombinant CPE binding protein tagged
470 with mCherry as a reporter for visualization of CPE on spermatocyte plasma membranes. The
471 mushroom-derived protein of the aegerolysin family pleurotolysin A2 (PlyA2) was shown to
472 specifically bind to CPE and was demonstrated to be a versatile tool for visualizing CPE in live
473 *Drosophila* tissues [39]. We have reevaluated the efficacy of recombinant PlyA2-mCherry
474 proteins in detecting endogenous CPE on live spermatocyte membranes. The wild type and *cpes*
475 mutant spermatocytes were treated with 10 μg/ml of PlyA2-mCherry in M3 insect media for 1hour
476 at room temperature, washed with fresh M3 media, and imaged on an Andor spinning disk confocal
477 microscope. As shown in Fig.6A-D, PlyA2-mCherry specifically bound to the plasma membranes
478 of wild type spermatocytes but not to the *cpes* mutant spermatocytes showing specificity of this
479 protein binding to CPE. Interestingly, PlyA2-mCherry was endocytosed in wild type
480 spermatocytes (Fig.6). To determine the nature of these endosomes where CPE is enriched, we
481 have performed live imaging on spermatocytes expressing endogenous EYFP-MYC tagged Rab
482 proteins [40]. The small GTPases Rab4, Rab7 and Rab11 were shown to mark early, late and
483 recycling endosomes respectively [41-43] while Rab6 was shown to be associated with the Golgi
484 membranes [44]. The spermatocytes expressing individual EYFP-Rab proteins were treated with
485 recombinant PlyA2-mCherry and imaged. As shown in Fig.6G, M and P, PlyA2-mCherry
486 colocalizes with Rab4, Rab7 and some of the Rab11 endosomes respectively. However, PlyA2-
487 mCherry containing structures did not colocalize with Rab 6 positive Golgi membranes (Fig.6J).
488 These results suggested that CPE on spermatocyte plasma membranes is actively targeted to the
489 endocytic pathway. We next wondered whether endosomes carrying CPE migrate to cleaveage
490 furrows during meiosis cytokinesis. EYFP-Rab 7 and EYFP-Rab11 were strongly expressed in

491 spermatocytes compared to Rab4 and therefore we followed their dynamics during meiosis
492 cytokinesis. Strikingly, as shown in Fig.7A-F, & Movie.S10, PlyA2-mCherry containing Rab7
493 positive endosomes were actively targetted to cleavage furrows. Similar EYFP-Rab7 localization
494 was seen in intact cysts (Fig.7G-I). The PlyA2-mCherry also colocalized to some of the EYFP-
495 Rab11 recycling endosomes which in turn localized to ingressing membranes at the cleavage
496 furrow (Fig.7J-O and Movie S11). Overall, the endocytosis of CPE and targeting to the ingressing
497 cleavage furrows via Rab7 and Rab11 endosomes indicates their importance in delivery of lipids
498 to the ingressing membranes of the furrow and coordination of this event with proper spindle
499 behaviour and meiosis cytokinesis.

500 ***Fig.6.Ceramide phosphoethanolamine (CPE) localizes to plasma membrane and endosomes.***
501 *(A-D) Live spermatocytes were incubated with purified PlyA2-mCherry (10 μg/ml) for 30 min*
502 *followed by washes with M3 insect media (2x) and imaged using spinning disk confocal*
503 *microscopy. (A and B) w^{1118} spemratocytes, (C and D) cpes spermatocytes. (E-P) Live*
504 *spermatocytes expressing endogenous EYFP tagged Rab proteins were incubated with PlyA2-*
505 *mCherry for one hour followed by washes with M3 insect media (2x) and imaged using spinning*
506 *disk confocal microscopy. (E-G) EYFP-Rab4 spermatocytes, (H-J) EYFP-Rab6 spermatocytes,*
507 *(K-M) EYFP-Rab7 spermatocytes, (N-P) EYFP-Rab11 spermatocytes. Arrow heads indicates*
508 *colocalizing structures.*

509 ***Fig.7. CPE containing endosomes translocate to cleavage furrows during male meiosis***
510 ***cytokinesis.*** *(A-F) The EYFP-Rab7 expressing spermatocytes were treated with PlyA2-mCherry*
511 *and snapshots of spermatocytes undergoing meiosis I cytokinesis were shown. (A-C) Horizontal*
512 *view of one z slice was shown (D-F) Cross sectional view of a spermatocyte undergoing*
513 *cytokinesis, maximum intensity projection image was shown. (G-I) Localization of EYFP-Rab7 in*

514 *intact cysts where spermatocytes are encapsulated by cyst cells. Horizontal view of a single z slice*
515 *was shown. (J-O) EYFP-Rab11 expressing spermatocytes were treated with PlyA2-mCherry and*
516 *meiosis I cytokinesis was imaged (J-L) Horizontal view of single z slice was shown (M-O) Cross*
517 *sectional view, maximum intensity projection image was shown. White arrows indicate*
518 *colocalization and white arrow heads indicates lack of colocalization.*

519 **Discussion**

520 Plasma membrane expansion and ingression of the cytokinetic furrow still remains one of the least
521 understood horizons in the field of cell division [45]. We are only beginning to appreciate the
522 involvement of lipids in structural integrity, membrane expansion, and transmission of signals
523 during cytokinesis. PIP2 is the most studied lipid in cytokinesis and has been shown to localize to
524 the cleavage furrow during ingression. In addition to PIP2, cholesterol, very long chain fatty acids
525 and sphingolipids have also been associated with cytokinesis [46] [10, 12]. In mitotic cells, PIP2
526 accumulation at the inner leaflet and subsequent recruitment of RhoGTPase (RhoA) was shown to
527 be coordinated with sphingomyelin rich domains on the outerleaflet [10]. However, it is unknown
528 if a similar mechanism exists in germ cells which have different characteristics and different lipid
529 composition. While mitotic cells were shown to accumulate classical sphingolipids with long to
530 very long acyl chains at midbodies [12], male germ cells accumulated complex sphingolipids with
531 verylong/ultralong chain polyunsaturared fatty acids (VLC-PUFAs) [13]. These differences in
532 sphingolipid composition with distinct biophysical properties between mitotic cells and male
533 meiotic cells point towards existence of distinct underlying mechanisms.

534 In this study, we show the sphingolipid composition of the major species in *Drosophila* testis for
535 the first time and demonstrate significant enrichment of unique CPE species containing
536 SPH_MUFA and SPD_SFA. Unlike mammalian testis, the *Drosophila* testis lacks significant

537 amounts of VLC-PUFA containing sphingolipids. However, due to conserved unsaturation in acyl
538 chains, it is likely that SPH_MUFA and SPD_SFA containing CPE could complement for VLC-
539 PUFA functions in *Drosophila* male germ cells. Glycosphingolipids with VLC/ULC PUFAs have
540 been shown to be required for mammalian male meiosis cytokinesis but their actual role has not
541 been delineated [13, 47, 48]. It is interesting to note that CPE mimics certain physical properties
542 of galactosylceramide (GalCer) a major sphingolipid in myelin sheath [49]. Previous studies have
543 shown that CPE has an essential role in axonal ensheathment and cortex glial plasma membrane
544 expansion in *Drosophila* [15, 50]. It was hypothesized that the axonal ensheathment in mammals
545 and *Drosophila* is based on similar physical process with different lipids [49]. We have previously
546 shown that sphingomyelin, a structural analogue of CPE, could rescues cortex glial membrane
547 defects in cpes mutants suggesting the head group is not as important as the tail group in glial
548 membranes. However, here we show that sphingomyelin could not rescue spermatogenesis defects
549 in *cpes* mutants alluding to the importance of the ethanolamine head group in spermatocytes.
550 Taken together, we could suggest that *Drosophila* CPE would have evolved to have both the
551 properties of mammalian glycosphingolipids and sphingomyelin to promote spermatogenesis and
552 glial ensheathment of neurons.
553 Phosphoinositides play critical role in cytokinesis particularly PIP2 was shown to be enriched at
554 the furrows and direcly binds to several proteins such as anillin, septins and MgcRacGAP to
555 mediate furrow stability [51, 52]. Unlike mitotic cells, PIP2 in male meiotic cells do not show
556 selective accumulation at cleavage furrows instead it is uniformly distributed throughout the
557 plasma membrane including at furrows ([37]and Fig.5E and Movie S4, S5 and S6). Interestingly
558 PIP2 hydrolysis and calcium release were shown to be required for cytokinesis in *Drosophila*
559 spermatocytes [37]. These observations suggests that PIP2 in meiotic cell has more broder role at

560 the plasma membrane and at furrows to promote cytokinesis. Interestingly, we show that the PIP3
561 binding protein Steppke (tGPH) localizes to cleavage furrows indicating a potential role for PIP3
562 during male meiosis cytokinesis. However, the accumulation of PIP3 to the cleavage furrows
563 occurs only in the intact cysts i.e, 16 interconnected spermatocytes wrapped up by two somatic
564 cyst cells suggesting the need for certain mechanical force. The role of PIP3 accumulation in the
565 male meiotic cleavage furrows is an open question and warrants future investigation. Interestingly,
566 recently it was shown that cytohesin Steppke reduces tissue tension by inhibiting the actomyosin
567 activity at adherens junctions in embryos [38]. Although broad accumulation of PIP2 to the plasma
568 membranes and PIP3 accumulation at the cleavage furrows was not altered in *cpes* mutants their
569 specific localization to membrane microdomains and their dynamics on functional alterations
570 cannot be ruled out. Sphingadienes with Δ 4.6 conjugated double bonds were previously identified
571 in *Drosophila*, *Manduca sexta*, and *Bombyx mori* [53-55], although their enrichment in the testis
572 was not known until now. However, normal sphingolipid synthesis and their degradation are
573 shown to be required for spermatogenesis [56, 57]. The sphingadiene sphingolipids were shown
574 to have inhibitory effects on AKT-dependent signaling [58] and downregulate Wnt signaling via
575 a PP2A/Akt/GSK3β pathway [59]. Accumulation of sphingadiene with saturated fatty acid
576 containing sphingolipids in the testis suggests that they could have a role in regulation of
577 PIP2/PIP3 mediated signaling *in vivo*. Consistent with this suggestion, total RNAseq results show
578 an upregulation of ERBB signaling in male germ cells. Apart from CPE_SPD_SFA the *Drosophila*
579 testis is also enriched in CPE_SPH_MUFA suggesting they could mediate distinct functions.
580 Lipids with unsaturated fatty acids mediate a number of biological functions [60]. It is widely
581 known that phospholipids with unsaturated fatty acids promote membrane fluidity and elasticity

582 [61, 62]. Sphingolipids with unsaturated fatty acids could thus provide unique biophysical
583 properties necessary for the membrane curvature requirements during meiosis cytokinesis.
584 Human genome encodes more than 60 Rab proteins and several of them including Rab1, Rab8,
585 Rab10, Rab14, Rab21, Rab24 and Rab35 were shown to localize to intercellular bridges. However,
586 most of the studies primarily focused on the recycling role of Rab11and Rab35 endosomes and
587 their effector proteins in cytokinesis [52]. Currently it is unknown if these endosomes are also
588 involved in delivery of specific plasma membrane drived lipids to the cleavage furrows. Our study
589 shows that there is an increased localization of CPE to the endosomal compartments in
590 spermatocytes. The CPE containing Rab7 and Rab11 endosomes are selectively targeted to
591 ingressing cleavage furrows suggesting possible addition of CPE rich membranes to the growing
592 furrows. Further investigations are needed to determine whether CPE enriched endosomes actively
593 participate in male meiosis cytokinesis, spermatid polarity and individualization by providing CPE
594 enriched membranes and or act as a signaling center to mediate spermatogenesis.

595 Materials and Methods

596 **Fly stocks**

597 tubulin-Gal4 (BDSC#5138), UAS-PLCdelta-PH-EGFP (BDSC#39693), tGPH (BDSC#8163),
598 Sqh-GFP.RLC (BDSC#57145), Sqh-mCherry.M (BDSC#59024), p(Ubi-p63E-Feo-mCherry)3
599 (BDSC#59277), bam-Gal4 [63], nos-Gal4 (BDSC#4937), chif-Gal4 (BDSC#13134), C587-Gal4
600 (BDSC#67747), EYFP-Rab4 (BDSC#62542), EYFP-Rab6 (BDSC#62544), EYFP-Rab7
601 (BDSC#62545), EYFP-Rab11(BDSC#62549), genomic CPES_V5tag [15], *cpes* mutants [15],
602 UAS-hSMS1 [15], dcert1[30], UAS CDase [31], UAS CPES active site mutants, UAS Aedes
603 CPES, UAS-Bombyx CPES, UAS-T. Urticae CPES (this study).

604 **Fly husbandry**

605 All *Drosophila* stocks were raised on standard fly food and maintained 25°C unless otherwise
606 mentioned. Due to increased lethality *cpes* mutants were raised at 18-21°C. Certain genetic
607 backgrounds increased pupal death in *cpes* mutants such as overexpression of UAS CDase, UAS-
608 PLCδ-PH-EGFP, *cpes*;*dcert*^{1} double mutants. In such cases we have separated 3rd instar larvae of
609 *cpes* mutants and allowed them to develop into the pupae. The testis were dissected before the
610 death of pupae and analyzed.

611 **Cloning of UAS-*Aedes egypty* CPES, UAS-*Bombyx Mori* CPES, UAS *Tetranechos Urticae***
612 **CPES**

613 The coding sequence for Aedes aegypti CPES (XM_021851518.1), Bombyx mori CPES
614 (XM_004923146.3) and Tetranychus urticae CPES (XM_015926572.2) were codon optimized
615 and synthesized by GenScript® and subcloned into pUAST vector. The clones were sent to
616 BestGene Inc for embryo injection service. The transgenic flies were balanced and crossed with
617 Gal4 drivers to conduct rescue experiments.

618 **Cloning of CPES active site mutant**

619 Two conserved aspartates in CPES active site were mutated to alanine using PCR based site
620 directed mutagenesis method as described by [64]. PCR was performed using pBluescript SK+
621 CPES_V5 clone as template with appropriate sense and antisense primers (Table S1) and Phusion
622 polymerase (NEB). The PCR product was digested with DpnI to remove templates followed by
623 transformation into DH5α competent cells. Plasmids were isolated from colonies grown in LB
624 media and screened by restriction digestion with appropriate restriction enzymes (Table S1) and
625 sequencing. The pBluescript SK+ CPES DD-AA clone was used as template to PCR amplify the
626 insert using appropriate primers (Table S1), restriction digested and cloned into pUAST vector.
627 The clones were confirmed with restriction digestion followed by DNA sequencing.

628 **Cloning, expression, and purification PlyA2mCherry**

629 Mushroom-derived aegerolysin PlyA2 was cloned, expressed and purified as described by [65].
630 Briefly, the coding sequence of PlyA2 (accession number AB777517) fused to mCherry at the C-
631 terminus was synthesized by GenScript®. The linker amino acid sequence between PlyA2 and
632 mCherry was VDGTAGPGSIAT. This clone was used as template to PCR amplify using
633 appropriate forward and reverse primers (Table S1) and cloned into p24 a vector at appropriate
634 restriction sites (Table S1). The clones were transformed into Escherichia coli strain BL-21 (DE3)
635 and single colony was inoculated in to 5ml of LB broth containing 50µg/ml kanamycin and grown
636 overnight in orbital shaker (200rpm) at 37°C. 2ml of overnight culture was inoculated into 250ml
637 of fresh LB broth containing kanamycin and grown at 37°C until the optical density reached to
638 0.6. Subsequently, the culture was incubated in cold (4°C) for 2 hours, followed by induction with
639 0.3mM isopropyl-B-D-thiogalactopyranoside and grown at 25°C in orbital shaker (200rpm)
640 overnight. The cells were harvested by centrifugation at 5,000g for 10min at 4°C and the pellet
641 was resuspended in binding buffer (20mM sodium phosphate buffer (pH 7.4), 500mM NaCl,
642 20mM imidazole) containing EDTA free protease inhibitor cocktail (Sigma, P8340). The cell
643 suspension (50 ml) was sonicated at 4°C (Cole-Parmer ultrasonic processor model CP130,) with
644 microprobe at an amplitude of 30 and on and off cycles of 10sec each for about 30 min to 1 hour.
645 The lysate was centrifuged at 10,000g for 10min to remove insoluble proteins and debris. To the
646 supernatant 1ml of 50% Ni-NTA agarose (Thermo Scientific) was added and incubated on end-to-
647 end rotor for 3 hours and the beads were collected on a column and washed with 30ml of binding
648 buffer and eluted with binding buffer containing 200mM imidazole. The fractions were dialysed
649 in 20mM sodium phosphate buffer 3 times (1L each) and the final protein was concentrated with
650 Amicon centriprep filter devices for volumes up to 15ml. The protein concentration was

651 determined using Bradford assay. The proteins were resuspended in 20% glycerol, aliquoted
652 (100µl) and stored at -80°C for future use.

653 **Testis squash preparation, phase contrast microscopy**

654 *Drosophila* testis squash preparations for phase-contrast microscopy and immunostaining were
655 performed as described by [16]. Briefly, young male (0-2 days old) testis were dissected (5 pairs)
656 in phosphate-buffered saline (PBS, 130 mM NaCl, 7mM Na2HPO4, 3mMH2PO4). The testis was
657 torn open on a slide at appropriate location with a pair of Black Anodized Steel needles (tip
658 diameter 0.0175mm) and a cover glass was gently placed without air bubbles. The slides were
659 directly observed under phase-contrast microscopy or snap frozen in liquid nitrogen for
660 immunostaining. After freezing the cover glass was removed from the slide with razor blade and
661 immersed in cold 99.5% ethanol and incubated in -20°C for 10 min. The slides were then fixed
662 with 4% paraformaldehyde (PFA) in PBS containing 0.1% Triton-X-100 (PBST) for 15 min.
663 Subsequently, the slides were washed with PBS and the area of squashed tissue was circled with a
664 hydrophobic barrier pen, permeabilized with PBST (30 min) and blocked with 5% normal goat
665 serum in PBST (1 hour at RT). Squashed tissues were incubated with primary (1µg in 100µl) and
666 secondary antibody (1:100 dilution) (8-12 hours each at 4°C in a moist chamber). Slides were
667 washed with PBST (3x 10 min each) after each antibody treatment, finally incubated with DAPI
668 solution (1:2000 dilution from 5mg/ml stock, Molecular Probes) and mounted with Vectashield
669 H1000 mounting media.

670 **Male fertility assay**

671 Male fertility assay was performed by setting up individual crosses with 1 male and 3 wild type
672 females. Each replicate involved 30 males and three independent replicates (total of 90 males)
673 were performed for each experiment.

674 **Immunostaining and confocal imaging**

675 *Drosophila* tissues were dissected and immunostained as described previously [15]. Briefly,
676 dissected testes were fixed with 4% PFA in 0.3% PBST for 1 hours at RT, washed (3x 10 min
677 each), permeabilized in 0.3% PBST (1 hour), blocked with 5% NGS (1hour) and incubated with
678 primary antibody (1:100 dilution or 1µg in 100µl of 5% NGS in PBST) overnight (8-12 hours).
679 Testes were washed with 0.3% PBST (3x10min each) and incubated with secondary antiobody
680 (1:100 dilution in 5%NGS in PBST). Testes were washed with PBST (3x 10 min each), stained
681 with DAPI (1:2000 dilution of 5mg/ml solution in PBST) for 15 min, and mounted with
682 Vectashield H1000 mounting medium. The slides were imaged on ZEISS confocal laser scanning
683 microscope LSM 780 or LSM880.

684 **Live cell imaging of meiotic cysts**

685 About 15-20 pairs of young (0-2days old) *Drosophila* testis were dissected in 600µl of insect cell
686 culture media (M3 media supplemented with heat inactivated FBS, Pen/Strep) in a glass well plate.
687 Testis were transferred to fresh a well with 400µl of media and tore open with a pair of Black
688 Anodized Steel needles (tip diameter 0.01mm) to release the cysts into media. This was repeated
689 until all the testes were torn opened, they were gently agitated so that all the cysts were released
690 into the media followed by removal of empty testis or debris from the media. The cysts were gently
691 washed with fresh 400µl media (2x), then transferred via pipetting into the middle of 35mm cover
692 glass bottom dish (Poly D-Lysine coated) and fresh media (max. 200µl) was gently added to the
693 cleft formed between cover glass and the dish. The cysts tend to move while handling but remains
694 settled on the cover glass and ideally remain in position while imaging. The intact cysts and cysts
695 that have lost their cyst cells could be distinguished in brightfield view. The cysts that are
696 beginning to undergo meiosis could be identified in brightfield view by looking at cell morphology

697 and differences in nucleus and spindle appearance. Cells beginning to undergo meiosis could also
698 be identified by Feo-mCherry which is localized to nucleus in interphase but translocates to cytosol
699 during prophase to anaphase. Prophase to anaphase cysts were identified using 25x water objective
700 and subsequently imaged using 63x water objective on a Leica Andor spinning disk confocal
701 microscope. The time lapse imaging was done at 2 min intervals with the z stacks (about 80 slices,
702 0.5µm per slice) at each time point for 60 to 90 min for completion of meiosis I cytokinesis. Laser
703 power and exposure times were preferably kept low to prevent bleaching and aberrant effects on
704 cytokinesis due to generation of free radicals.

705 **Sphingolipid estimation in fly tissues using Supercritical fluid chromatography**
706 **coupled to mass spectrometry (SFC/MS/MS)**

707 Sphingolipid estimation using supercritical fluid chromatography coupled to mass spectrometry
708 (SFC/MS/MS) was performed as described previously [15]. Lipids were extracted from heads,
709 ovary and testis samples as described [66, 67]. About 400 fly heads, about 250 pairs of ovaries and
710 about 250 pairs of testes were used for each biological replicate. Three independent replicates were
711 taken for each sample. For Figs.1 and 2 only testis alone samples were used whereas for Fig.4
712 whole male organ (testis, accessory glands, collecting ducts and ejaculation bulb) were used for
713 lipid extraction. Internal standards (ISTD) added to the tissues before extraction included 500 pmol
714 (20 µl) of Cer/Sph Mixture I (Avanti Polar Lipids LM-6002), and 1nmol of C12 Sphingosyl PE
715 (C17:1/C12:0) (Avanti Polar Lipids). Lipids from all samples were normalized to carbon content
716 (100µg/ml) and 100 µg/ml sample was diluted 10 times before injection for SFC. We have used
717 large-fragment MRM method for quantitation of amount per 100µg of carbon.

718 **Total RNA sequencing**

719 Three independent biological replicates were performed for each sample and about 200 pairs of
720 w^{1118} (WT 1-3), *cpes* mutant (KO 1-3) and Bam-Gal4>UAS CPES rescued (RES 1-3) fly testis
721 were dissected for each replicate. The testes were dissected in S2 cell culture media, washed with
722 PBS and RNA was extracted. Total RNA was extracted using Trizol method followed by DNAase
723 I treatment and purification using RNA Clean and Concentrator™-5 kit (Zymoresearch). A total
724 of 2µg of RNA was submitted to Novogene for total RNA seq. The RNA seq data was further
725 analyzed for differential gene expression and pathway analysis using Gene Set Enrichment
726 Aanalysis (GSEA). The gene sets specific for drosophilla were downloaded from
727 http://www.bioinformatics.org/go2msig/ and http://ge-lab.org/gskb/.

728 **Acknowledgments**

729 This study was funded by the intramural division of the National Cancer Institute, National
730 Institutes of Health (Division of Health and Human Services). The content of this publication does
731 not necessarily reflect the views or policies of the Department of Health and Human Services, nor
732 does mention of trade names, commercial products, or organizations imply endorsement by the
733 U.S. Government.
734 This work was partially supported by the Grant-in-Aid for Scientific Research on Innovative Areas
735 (17H06304) [T.B.] and a Grant-in-Aid for Scientific Research (B) (18H01800) [T.B.] from Japan
736 Society for the Promotion of Science (JSPS).

737 **Conflict of Interest Statement**

738 The authors declare no conflicts of interests.

739

740

741

742 # References

743 1. Fahy E, Subramaniam S, Murphy RC, Nishijima M, Raetz CR, Shimizu T, et al. Update of the
744 LIPID MAPS comprehensive classification system for lipids. J Lipid Res. 2009;50 Suppl:S9-14. Epub
745 2008/12/23. doi: 10.1194/jlr.R800095-JLR200. PubMed PMID: 19098281; PubMed Central
746 PMCID: PMCPMC2674711.
747 2. Harayama T, Riezman H. Understanding the diversity of membrane lipid composition. Nat
748 Rev Mol Cell Biol. 2018;19(5):281-96. Epub 2018/02/08. doi: 10.1038/nrm.2017.138. PubMed
749 PMID: 29410529.
750 3. Kutateladze TG. Translation of the phosphoinositide code by PI effectors. Nat Chem Biol.
751 2010;6(7):507-13. Epub 2010/06/19. doi: 10.1038/nchembio.390. PubMed PMID: 20559318;
752 PubMed Central PMCID: PMCPMC3182472.
753 4. Hunt AN, Skippen AJ, Koster G, Postle AD, Cockcroft S. Acyl chain-based molecular
754 selectivity for HL60 cellular phosphatidylinositol and of phosphatidylcholine by
755 phosphatidylinositol transfer protein alpha. Biochim Biophys Acta. 2004;1686(1-2):50-60. Epub
756 2004/11/04. doi: 10.1016/j.bbalip.2004.08.003. PubMed PMID: 15522822.
757 5. Shulga YV, Topham MK, Epand RM. Study of arachidonoyl specificity in two enzymes of
758 the PI cycle. J Mol Biol. 2011;409(2):101-12. Epub 2011/04/12. doi: 10.1016/j.jmb.2011.03.071.
759 PubMed PMID: 21477596; PubMed Central PMCID: PMCPMC3095698.
760 6. Schuhmacher M, Grasskamp AT, Barahtjan P, Wagner N, Lombardot B, Schuhmacher JS,
761 et al. Live-cell lipid biochemistry reveals a role of diacylglycerol side-chain composition for cellular
762 lipid dynamics and protein affinities. Proc Natl Acad Sci U S A. 2020;117(14):7729-38. Epub
763 2020/03/28. doi: 10.1073/pnas.1912684117. PubMed PMID: 32213584; PubMed Central PMCID:
764 PMCPMC7149225.
765 7. Rodriguez-Gallardo S, Kurokawa K, Sabido-Bozo S, Cortes-Gomez A, Ikeda A, Zoni V, et al.
766 Ceramide chain length-dependent protein sorting into selective endoplasmic reticulum exit sites.
767 Sci Adv. 2020;6(50). Epub 2020/12/15. doi: 10.1126/sciadv.aba8237. PubMed PMID: 33310842;
768 PubMed Central PMCID: PMCPMC7732199.
769 8. Contreras FX, Ernst AM, Haberkant P, Bjorkholm P, Lindahl E, Gonen B, et al. Molecular
770 recognition of a single sphingolipid species by a protein's transmembrane domain. Nature.
771 2012;481(7382):525-9. Epub 2012/01/11. doi: 10.1038/nature10742. PubMed PMID: 22230960.
772 9. Li R. Cytokinesis in development and disease: variations on a common theme. Cell Mol
773 Life Sci. 2007;64(23):3044-58. Epub 2007/09/21. doi: 10.1007/s00018-007-7285-6. PubMed
774 PMID: 17882379.
775 10. Abe M, Makino A, Hullin-Matsuda F, Kamijo K, Ohno-Iwashita Y, Hanada K, et al. A role for
776 sphingomyelin-rich lipid domains in the accumulation of phosphatidylinositol-4,5-bisphosphate
777 to the cleavage furrow during cytokinesis. Mol Cell Biol. 2012;32(8):1396-407. Epub 2012/02/15.
778 doi: 10.1128/MCB.06113-11. PubMed PMID: 22331463; PubMed Central PMCID:
779 PMCPMC3318597.
780 11. Atilla-Gokcumen GE, Bedigian AV, Sasse S, Eggert US. Inhibition of glycosphingolipid
781 biosynthesis induces cytokinesis failure. J Am Chem Soc. 2011;133(26):10010-3. Epub
782 2011/06/15. doi: 10.1021/ja202804b. PubMed PMID: 21668028; PubMed Central PMCID:
783 PMCPMC3131740.

784 12. Atilla-Gokcumen GE, Muro E, Relat-Goberna J, Sasse S, Bedigian A, Coughlin ML, et al.
785 Dividing cells regulate their lipid composition and localization. Cell. 2014;156(3):428-39. Epub
786 2014/01/28. doi: 10.1016/j.cell.2013.12.015. PubMed PMID: 24462247; PubMed Central PMCID:
787 PMCPMC3909459.
788 13. Rabionet M, Bayerle A, Jennemann R, Heid H, Fuchser J, Marsching C, et al. Male meiotic
789 cytokinesis requires ceramide synthase 3-dependent sphingolipids with unique membrane
790 anchors. Hum Mol Genet. 2015;24(17):4792-808. Epub 2015/06/06. doi: 10.1093/hmg/ddv204.
791 PubMed PMID: 26045466.
792 14. Robinson BS, Johnson DW, Poulos A. Novel molecular species of sphingomyelin containing
793 2-hydroxylated polyenoic very-long-chain fatty acids in mammalian testes and spermatozoa. J
794 Biol Chem. 1992;267(3):1746-51. Epub 1992/01/25. PubMed PMID: 1730716.
795 15. Kunduri G, Turner-Evans D, Konya Y, Izumi Y, Nagashima K, Lockett S, et al. Defective
796 cortex glia plasma membrane structure underlies light-induced epilepsy in cpes mutants. Proc
797 Natl Acad Sci U S A. 2018;115(38):E8919-E28. Epub 2018/09/07. doi: 10.1073/pnas.1808463115.
798 PubMed PMID: 30185559; PubMed Central PMCID: PMCPMC6156639.
799 16. Sitaram P, Hainline SG, Lee LA. Cytological analysis of spermatogenesis: live and fixed
800 preparations of Drosophila testes. J Vis Exp. 2014;(83):e51058. Epub 2014/01/30. doi:
801 10.3791/51058. PubMed PMID: 24473184; PubMed Central PMCID: PMCPMC4089415.
802 17. Gonzalez C, Casal J, Ripoll P. Relationship between chromosome content and nuclear
803 diameter in early spermatids of Drosophila melanogaster. Genet Res. 1989;54(3):205-12. Epub
804 1989/12/01. doi: 10.1017/s0016672300028664. PubMed PMID: 2515989.
805 18. Fuller MT. Spermatogenesis. In: Bate MaM-A, A., editor. The Development of Drosophila.
806 Cold Spring Harbor, NY: Cold Spring Harbor Laboratory Press; 1993. p. 71-147.
807 19. Basu J, Williams BC, Li Z, Williams EV, Goldberg ML. Depletion of a Drosophila homolog of
808 yeast Sup35p disrupts spindle assembly, chromosome segregation, and cytokinesis during male
809 meiosis. Cell Motil Cytoskeleton. 1998;39(4):286-302. Epub 1998/04/29. doi: 10.1002/(SICI)1097-
810 0169(1998)39:4<286::AID-CM4>3.0.CO;2-1. PubMed PMID: 9556329.
811 20. Carmena M, Riparbelli MG, Minestrini G, Tavares AM, Adams R, Callaini G, et al.
812 Drosophila polo kinase is required for cytokinesis. J Cell Biol. 1998;143(3):659-71. Epub
813 1998/11/13. doi: 10.1083/jcb.143.3.659. PubMed PMID: 9813088; PubMed Central PMCID:
814 PMCPMC2148135.
815 21. Castrillon DH, Wasserman SA. Diaphanous is required for cytokinesis in Drosophila and
816 shares domains of similarity with the products of the limb deformity gene. Development.
817 1994;120(12):3367-77. Epub 1994/12/01. PubMed PMID: 7821209.
818 22. Giansanti MG, Bonaccorsi S, Williams B, Williams EV, Santolamazza C, Goldberg ML, et al.
819 Cooperative interactions between the central spindle and the contractile ring during Drosophila
820 cytokinesis. Genes Dev. 1998;12(3):396-410. Epub 1998/02/28. doi: 10.1101/gad.12.3.396.
821 PubMed PMID: 9450933; PubMed Central PMCID: PMCPMC316479.
822 23. Gunsalus KC, Bonaccorsi S, Williams E, Verni F, Gatti M, Goldberg ML. Mutations in
823 twinstar, a Drosophila gene encoding a cofilin/ADF homologue, result in defects in centrosome
824 migration and cytokinesis. J Cell Biol. 1995;131(5):1243-59. Epub 1995/12/01. doi:
825 10.1083/jcb.131.5.1243. PubMed PMID: 8522587; PubMed Central PMCID: PMCPMC2120640.
826 24. Williams BC, Riedy MF, Williams EV, Gatti M, Goldberg ML. The Drosophila kinesin-like
827 protein KLP3A is a midbody component required for central spindle assembly and initiation of

828 cytokinesis. J Cell Biol. 1995;129(3):709-23. Epub 1995/05/01. doi: 10.1083/jcb.129.3.709.
829 PubMed PMID: 7730406; PubMed Central PMCID: PMCPMC2120429.
830 25. Steinhauer J. Separating from the pack: Molecular mechanisms of Drosophila spermatid
831 individualization. Spermatogenesis. 2015;5(2):e1041345. Epub 2015/09/29. doi:
832 10.1080/21565562.2015.1041345. PubMed PMID: 26413413; PubMed Central PMCID:
833 PMCPMC4581072.
834 26. Arama E, Agapite J, Steller H. Caspase activity and a specific cytochrome C are required
835 for sperm differentiation in Drosophila. Dev Cell. 2003;4(5):687-97. Epub 2003/05/10. doi:
836 10.1016/s1534-5807(03)00120-5. PubMed PMID: 12737804.
837 27. Vacaru AM, van den Dikkenberg J, Ternes P, Holthuis JC. Ceramide phosphoethanolamine
838 biosynthesis in Drosophila is mediated by a unique ethanolamine phosphotransferase in the Golgi
839 lumen. J Biol Chem. 2013;288(16):11520-30. Epub 2013/03/02. doi: 10.1074/jbc.M113.460972.
840 PubMed PMID: 23449981; PubMed Central PMCID: PMCPMC3630839.
841 28. Henneberry AL, Wright MM, McMaster CR. The major sites of cellular phospholipid
842 synthesis and molecular determinants of Fatty Acid and lipid head group specificity. Mol Biol Cell.
843 2002;13(9):3148-61. Epub 2002/09/11. doi: 10.1091/mbc.01-11-0540. PubMed PMID:
844 12221122; PubMed Central PMCID: PMCPMC124149.
845 29. Williams JG, McMaster CR. Scanning alanine mutagenesis of the CDP-alcohol
846 phosphotransferase motif of Saccharomyces cerevisiae cholinephosphotransferase. J Biol Chem.
847 1998;273(22):13482-7. Epub 1998/06/05. doi: 10.1074/jbc.273.22.13482. PubMed PMID:
848 9593682.
849 30. Rao RP, Yuan C, Allegood JC, Rawat SS, Edwards MB, Wang X, et al. Ceramide transfer
850 protein function is essential for normal oxidative stress response and lifespan. Proc Natl Acad Sci
851 U S A. 2007;104(27):11364-9. Epub 2007/06/27. doi: 10.1073/pnas.0705049104. PubMed PMID:
852 17592126; PubMed Central PMCID: PMCPMC1899189.
853 31. Acharya U, Patel S, Koundakjian E, Nagashima K, Han X, Acharya JK. Modulating
854 sphingolipid biosynthetic pathway rescues photoreceptor degeneration. Science.
855 2003;299(5613):1740-3. Epub 2003/03/15. doi: 10.1126/science.1080549. PubMed PMID:
856 12637747.
857 32. Wang H, Brust-Mascher I, Scholey JM. The microtubule cross-linker Feo controls the
858 midzone stability, motor composition, and elongation of the anaphase B spindle in Drosophila
859 embryos. Mol Biol Cell. 2015;26(8):1452-62. Epub 2015/02/20. doi: 10.1091/mbc.E14-12-1631.
860 PubMed PMID: 25694445; PubMed Central PMCID: PMCPMC4395126.
861 33. Royou A, Field C, Sisson JC, Sullivan W, Karess R. Reassessing the role and dynamics of
862 nonmuscle myosin II during furrow formation in early Drosophila embryos. Mol Biol Cell.
863 2004;15(2):838-50. Epub 2003/12/06. doi: 10.1091/mbc.e03-06-0440. PubMed PMID:
864 14657248; PubMed Central PMCID: PMCPMC329397.
865 34. Brill JA, Wong R, Wilde A. Phosphoinositide function in cytokinesis. Curr Biol.
866 2011;21(22):R930-4. Epub 2011/11/26. doi: 10.1016/j.cub.2011.10.001. PubMed PMID:
867 22115464.
868 35. Britton JS, Lockwood WK, Li L, Cohen SM, Edgar BA. Drosophila's insulin/PI3-kinase
869 pathway coordinates cellular metabolism with nutritional conditions. Dev Cell. 2002;2(2):239-49.
870 Epub 2002/02/08. doi: 10.1016/s1534-5807(02)00117-x. PubMed PMID: 11832249.

871 36. Verstreken P, Ohyama T, Haueter C, Habets RL, Lin YQ, Swan LE, et al. Tweek, an
872 evolutionarily conserved protein, is required for synaptic vesicle recycling. Neuron.
873 2009;63(2):203-15. Epub 2009/07/31. doi: 10.1016/j.neuron.2009.06.017. PubMed PMID:
874 19640479; PubMed Central PMCID: PMCPMC2759194.
875 37. Wong R, Hadjiyanni I, Wei HC, Polevoy G, McBride R, Sem KP, et al. PIP2 hydrolysis and
876 calcium release are required for cytokinesis in Drosophila spermatocytes. Curr Biol.
877 2005;15(15):1401-6. Epub 2005/08/09. doi: 10.1016/j.cub.2005.06.060. PubMed PMID:
878 16085493.
879 38. West JJ, Zulueta-Coarasa T, Maier JA, Lee DM, Bruce AEE, Fernandez-Gonzalez R, et al. An
880 Actomyosin-Arf-GEF Negative Feedback Loop for Tissue Elongation under Stress. Curr Biol.
881 2017;27(15):2260-70 e5. Epub 2017/07/25. doi: 10.1016/j.cub.2017.06.038. PubMed PMID:
882 28736167.
883 39. Bhat HB, Ishitsuka R, Inaba T, Murate M, Abe M, Makino A, et al. Evaluation of
884 aegerolysins as novel tools to detect and visualize ceramide phosphoethanolamine, a major
885 sphingolipid in invertebrates. FASEB J. 2015;29(9):3920-34. Epub 2015/06/11. doi: 10.1096/fj.15-
886 272112. PubMed PMID: 26060215.
887 40. Dunst S, Kazimiers T, von Zadow F, Jambor H, Sagner A, Brankatschk B, et al. Endogenously
888 tagged rab proteins: a resource to study membrane trafficking in Drosophila. Dev Cell.
889 2015;33(3):351-65. Epub 2015/05/06. doi: 10.1016/j.devcel.2015.03.022. PubMed PMID:
890 25942626; PubMed Central PMCID: PMCPMC4431667.
891 41. Van Der Sluijs P, Hull M, Zahraoui A, Tavitian A, Goud B, Mellman I. The small GTP-binding
892 protein rab4 is associated with early endosomes. Proc Natl Acad Sci U S A. 1991;88(14):6313-7.
893 Epub 1991/07/15. doi: 10.1073/pnas.88.14.6313. PubMed PMID: 1906178; PubMed Central
894 PMCID: PMCPMC52073.
895 42. Pfeffer SR. Rab GTPases: specifying and deciphering organelle identity and function.
896 Trends Cell Biol. 2001;11(12):487-91. Epub 2001/11/24. doi: 10.1016/s0962-8924(01)02147-x.
897 PubMed PMID: 11719054.
898 43. Albertson R, Riggs B, Sullivan W. Membrane traffic: a driving force in cytokinesis. Trends
899 Cell Biol. 2005;15(2):92-101. Epub 2005/02/08. doi: 10.1016/j.tcb.2004.12.008. PubMed PMID:
900 15695096.
901 44. Echard A, Jollivet F, Martinez O, Lacapere JJ, Rousselet A, Janoueix-Lerosey I, et al.
902 Interaction of a Golgi-associated kinesin-like protein with Rab6. Science. 1998;279(5350):580-5.
903 Epub 1998/02/07. doi: 10.1126/science.279.5350.580. PubMed PMID: 9438855.
904 45. Pollard TD. Nine unanswered questions about cytokinesis. J Cell Biol. 2017;216(10):3007-
905 16. Epub 2017/08/16. doi: 10.1083/jcb.201612068. PubMed PMID: 28807993; PubMed Central
906 PMCID: PMCPMC5626534.
907 46. Ng MM, Chang F, Burgess DR. Movement of membrane domains and requirement of
908 membrane signaling molecules for cytokinesis. Dev Cell. 2005;9(6):781-90. Epub 2005/12/06.
909 doi: 10.1016/j.devcel.2005.11.002. PubMed PMID: 16326390.
910 47. Rabionet M, van der Spoel AC, Chuang CC, von Tumpling-Radosta B, Litjens M,
911 Bouwmeester D, et al. Male germ cells require polyenoic sphingolipids with complex
912 glycosylation for completion of meiosis: a link to ceramide synthase-3. J Biol Chem.
913 2008;283(19):13357-69. Epub 2008/03/01. doi: 10.1074/jbc.M800870200. PubMed PMID:
914 18308723; PubMed Central PMCID: PMCPMC2442322.

915 48. Wittmann A, Grimm MO, Scherthan H, Horsch M, Beckers J, Fuchs H, et al. Sphingomyelin
916 Synthase 1 Is Essential for Male Fertility in Mice. PLoS One. 2016;11(10):e0164298. Epub
917 2016/10/28. doi: 10.1371/journal.pone.0164298. PubMed PMID: 27788151; PubMed Central
918 PMCID: PMCPMC5082796.
919 49. Inaba T, Murate M, Tomishige N, Lee YF, Hullin-Matsuda F, Pollet B, et al. Formation of
920 tubules and helical ribbons by ceramide phosphoethanolamine-containing membranes. Sci Rep.
921 2019;9(1):5812. Epub 2019/04/11. doi: 10.1038/s41598-019-42247-1. PubMed PMID: 30967612;
922 PubMed Central PMCID: PMCPMC6456502.
923 50. Ghosh A, Kling T, Snaidero N, Sampaio JL, Shevchenko A, Gras H, et al. A global in vivo
924 Drosophila RNAi screen identifies a key role of ceramide phosphoethanolamine for glial
925 ensheathment of axons. PLoS Genet. 2013;9(12):e1003980. Epub 2013/12/19. doi:
926 10.1371/journal.pgen.1003980. PubMed PMID: 24348263; PubMed Central PMCID:
927 PMCPMC3861124.
928 51. Schink KO, Tan KW, Stenmark H. Phosphoinositides in Control of Membrane Dynamics.
929 Annu Rev Cell Dev Biol. 2016;32:143-71. Epub 2016/09/01. doi: 10.1146/annurev-cellbio-
930 111315-125349. PubMed PMID: 27576122.
931 52. Fremont S, Echard A. Membrane Traffic in the Late Steps of Cytokinesis. Curr Biol.
932 2018;28(8):R458-R70. Epub 2018/04/25. doi: 10.1016/j.cub.2018.01.019. PubMed PMID:
933 29689230.
934 53. Abeytunga DT, Glick JJ, Gibson NJ, Oland LA, Somogyi A, Wysocki VH, et al. Presence of
935 unsaturated sphingomyelins and changes in their composition during the life cycle of the moth
936 Manduca sexta. J Lipid Res. 2004;45(7):1221-31. Epub 2004/04/23. doi: 10.1194/jlr.M300392-
937 JLR200. PubMed PMID: 15102888.
938 54. Fyrst H, Zhang X, Herr DR, Byun HS, Bittman R, Phan VH, et al. Identification and
939 characterization by electrospray mass spectrometry of endogenous Drosophila sphingadienes. J
940 Lipid Res. 2008;49(3):597-606. Epub 2007/12/25. doi: 10.1194/jlr.M700414-JLR200. PubMed
941 PMID: 18156591.
942 55. Kwon HC, Lee KC, Cho OR, Jung IY, Cho SY, Kim SY, et al. Sphingolipids from Bombycis
943 Corpus 101A and their neurotrophic effects. J Nat Prod. 2003;66(4):466-9. Epub 2003/04/26. doi:
944 10.1021/np0204491. PubMed PMID: 12713394.
945 56. Basu J, Li Z. The Des-1 protein, required for central spindle assembly and cytokinesis, is
946 associated with mitochondria along the meiotic spindle apparatus and with the contractile ring
947 during male meiosis in Drosophila melanogaster. Mol Gen Genet. 1998;259(6):664-73. Epub
948 1998/11/18. doi: 10.1007/s004380050861. PubMed PMID: 9819060.
949 57. Phan VH, Herr DR, Panton D, Fyrst H, Saba JD, Harris GL. Disruption of sphingolipid
950 metabolism elicits apoptosis-associated reproductive defects in Drosophila. Dev Biol.
951 2007;309(2):329-41. Epub 2007/08/21. doi: 10.1016/j.ydbio.2007.07.021. PubMed PMID:
952 17706961; PubMed Central PMCID: PMCPMC2094363.
953 58. Fyrst H, Oskouian B, Bandhuvula P, Gong Y, Byun HS, Bittman R, et al. Natural
954 sphingadienes inhibit Akt-dependent signaling and prevent intestinal tumorigenesis. Cancer Res.
955 2009;69(24):9457-64. Epub 2009/11/26. doi: 10.1158/0008-5472.CAN-09-2341. PubMed PMID:
956 19934323; PubMed Central PMCID: PMCPMC2795098.
957 59. Kumar A, Pandurangan AK, Lu F, Fyrst H, Zhang M, Byun HS, et al. Chemopreventive
958 sphingadienes downregulate Wnt signaling via a PP2A/Akt/GSK3beta pathway in colon cancer.

959 Carcinogenesis. 2012;33(9):1726-35. Epub 2012/05/15. doi: 10.1093/carcin/bgs174. PubMed
960 PMID: 22581840; PubMed Central PMCID: PMCPMC3514901.
961 60. Wiktorowska-Owczarek A, Berezinska M, Nowak JZ. PUFAs: Structures, Metabolism and
962 Functions. Adv Clin Exp Med. 2015;24(6):931-41. Epub 2016/01/16. doi: 10.17219/acem/31243.
963 PubMed PMID: 26771963.
964 61. Feller SE, Gawrisch K. Properties of docosahexaenoic-acid-containing lipids and their
965 influence on the function of rhodopsin. Curr Opin Struct Biol. 2005;15(4):416-22. Epub
966 2005/07/26. doi: 10.1016/j.sbi.2005.07.002. PubMed PMID: 16039844.
967 62. Rawicz W, Olbrich KC, McIntosh T, Needham D, Evans E. Effect of chain length and
968 unsaturation on elasticity of lipid bilayers. Biophys J. 2000;79(1):328-39. Epub 2000/06/27. doi:
969 10.1016/S0006-3495(00)76295-3. PubMed PMID: 10866959; PubMed Central PMCID:
970 PMCPMC1300937.
971 63. Chen D, McKearin DM. A discrete transcriptional silencer in the bam gene determines
972 asymmetric division of the Drosophila germline stem cell. Development. 2003;130(6):1159-70.
973 Epub 2003/02/07. doi: 10.1242/dev.00325. PubMed PMID: 12571107.
974 64. Weiner MP, Costa GL, Schoettlin W, Cline J, Mathur E, Bauer JC. Site-directed mutagenesis
975 of double-stranded DNA by the polymerase chain reaction. Gene. 1994;151(1-2):119-23. Epub
976 1994/12/30. doi: 10.1016/0378-1119(94)90641-6. PubMed PMID: 7828859.
977 65. Bhat HB, Kishimoto T, Abe M, Makino A, Inaba T, Murate M, et al. Binding of a
978 pleurotolysin ortholog from Pleurotus eryngii to sphingomyelin and cholesterol-rich membrane
979 domains. J Lipid Res. 2013;54(10):2933-43. Epub 2013/08/07. doi: 10.1194/jlr.D041731. PubMed
980 PMID: 23918047; PubMed Central PMCID: PMCPMC3770106.
981 66. Fyrst H, Herr DR, Harris GL, Saba JD. Characterization of free endogenous C14 and C16
982 sphingoid bases from Drosophila melanogaster. J Lipid Res. 2004;45(1):54-62. Epub 2003/09/18.
983 doi: 10.1194/jlr.M300005-JLR200. PubMed PMID: 13130120.
984 67. Merrill AH, Jr., Sullards MC, Allegood JC, Kelly S, Wang E. Sphingolipidomics: high-
985 throughput, structure-specific, and quantitative analysis of sphingolipids by liquid
986 chromatography tandem mass spectrometry. Methods. 2005;36(2):207-24. Epub 2005/05/17.
987 doi: 10.1016/j.ymeth.2005.01.009. PubMed PMID: 15894491.
988

989

Figure 1
Kunduri et al., 2021

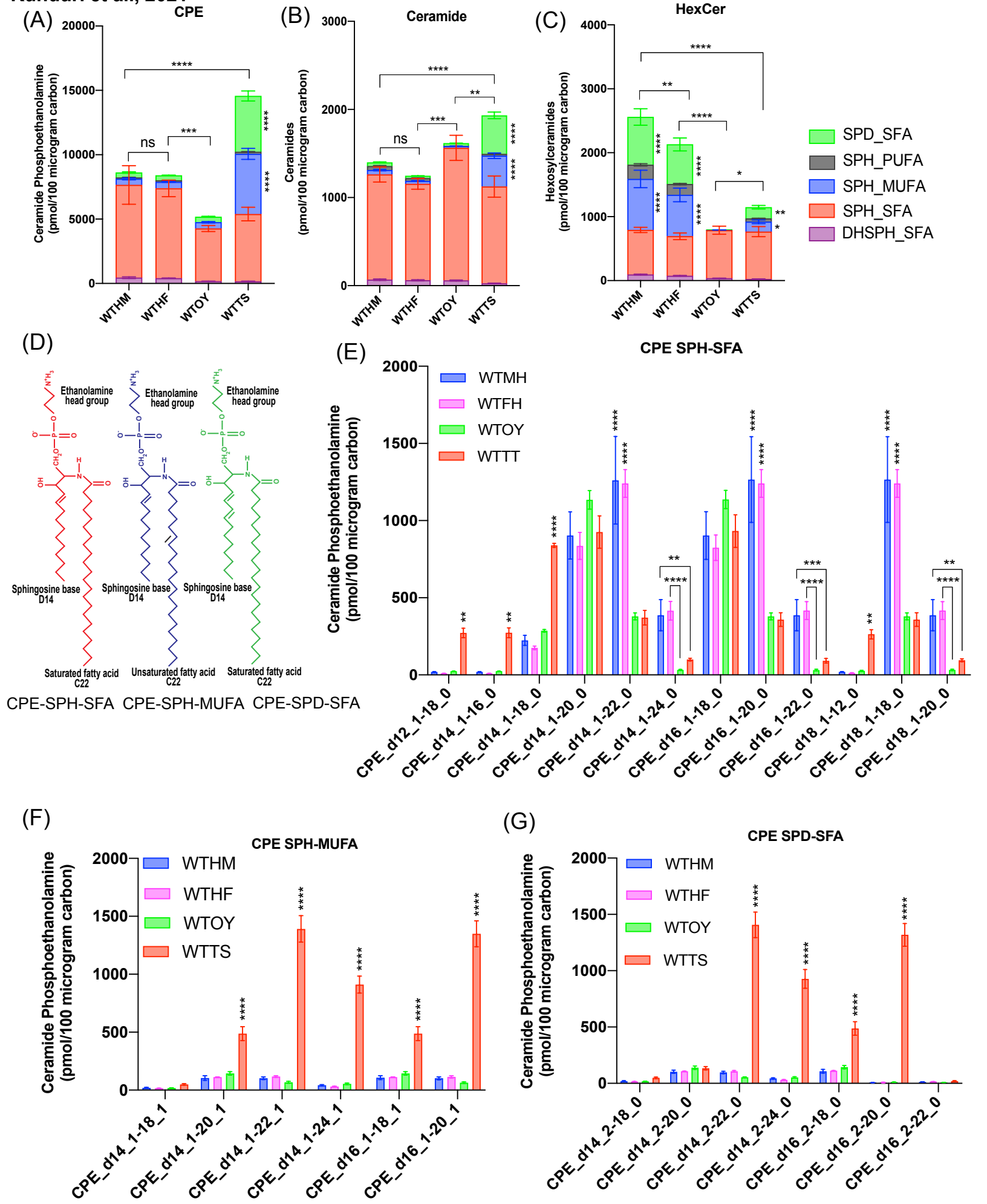

Figure 2
Kunduri et al., 2021

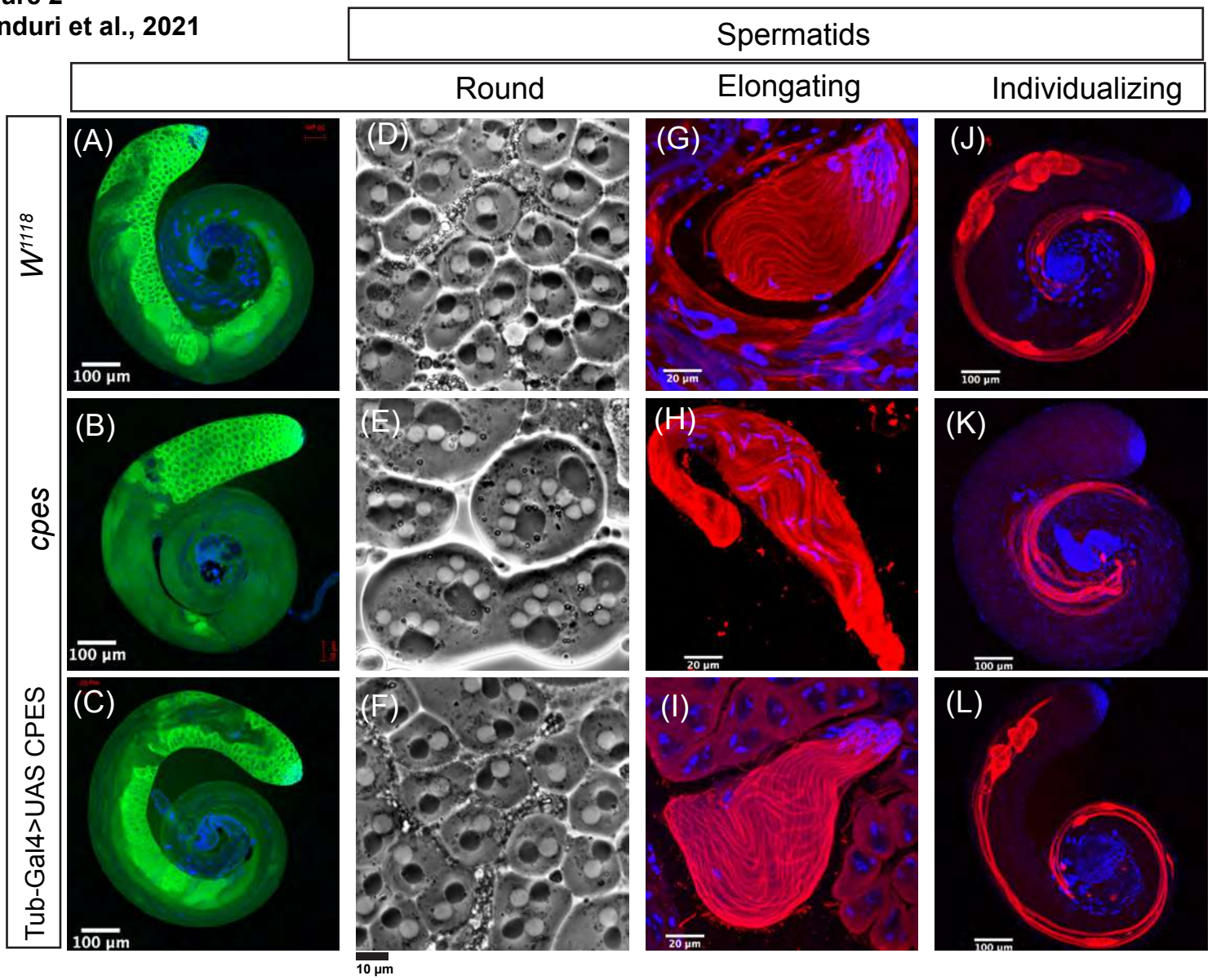

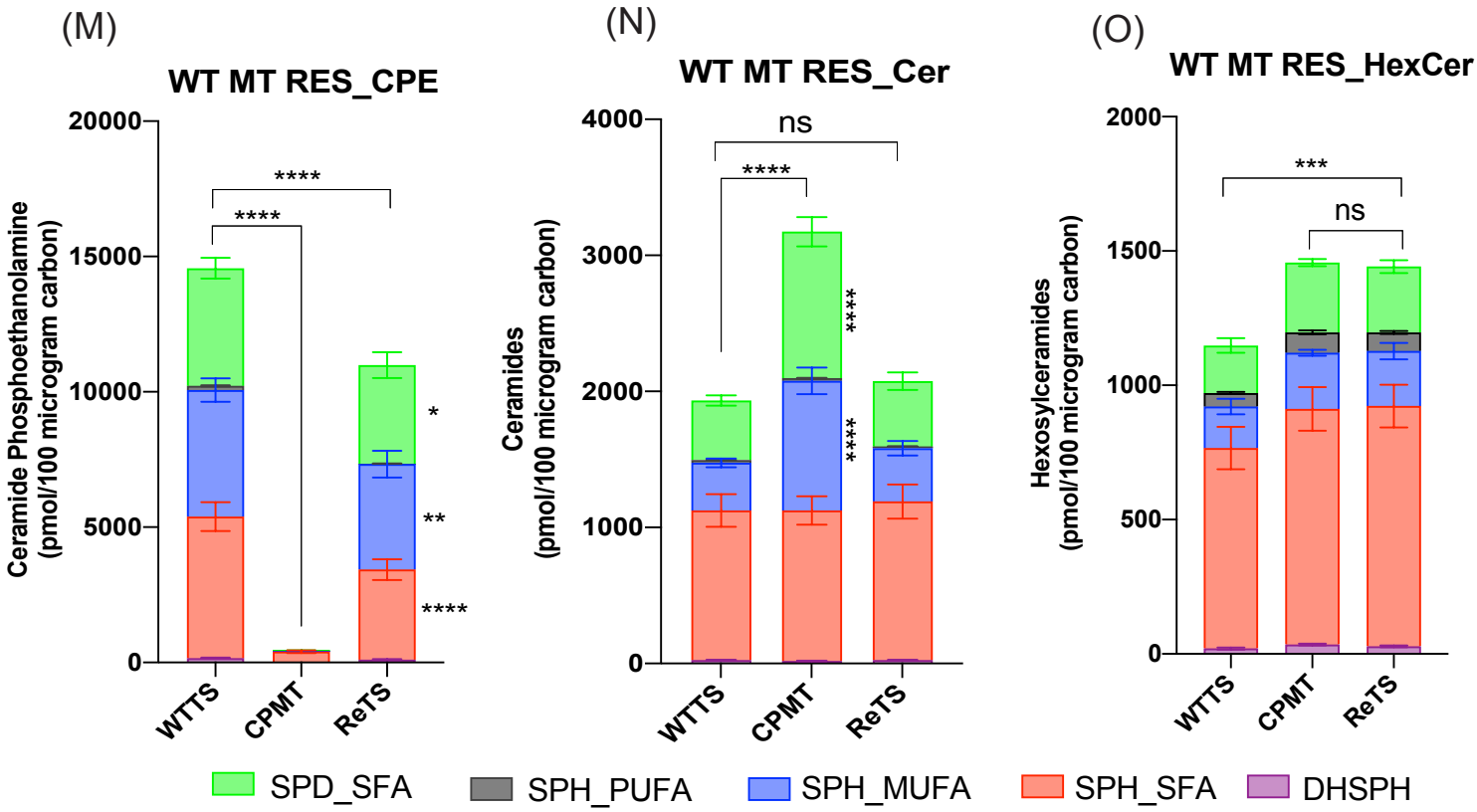

Figure 3
Kunduri et al., 2021

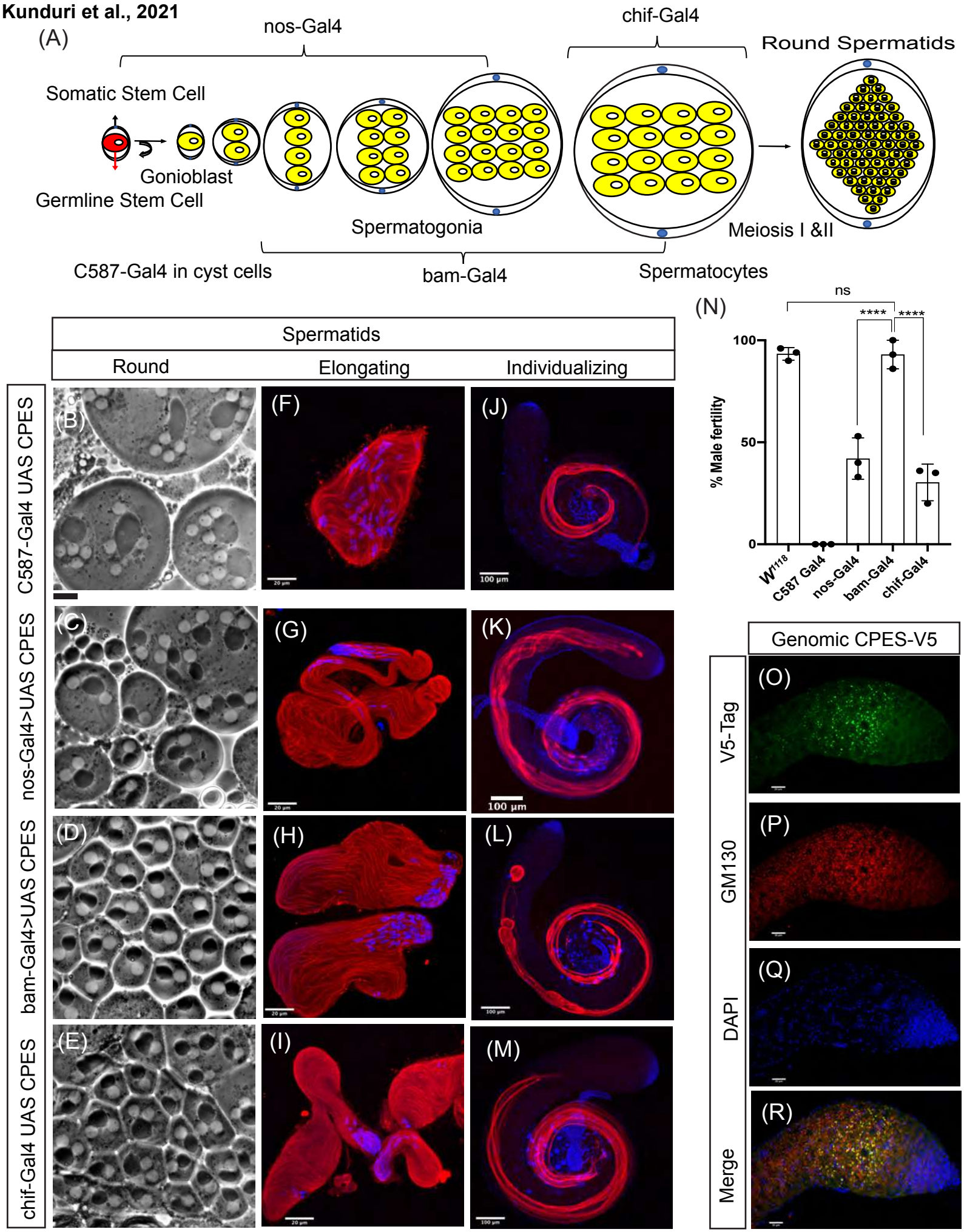

Figure 4
Kunduri et al., 2021

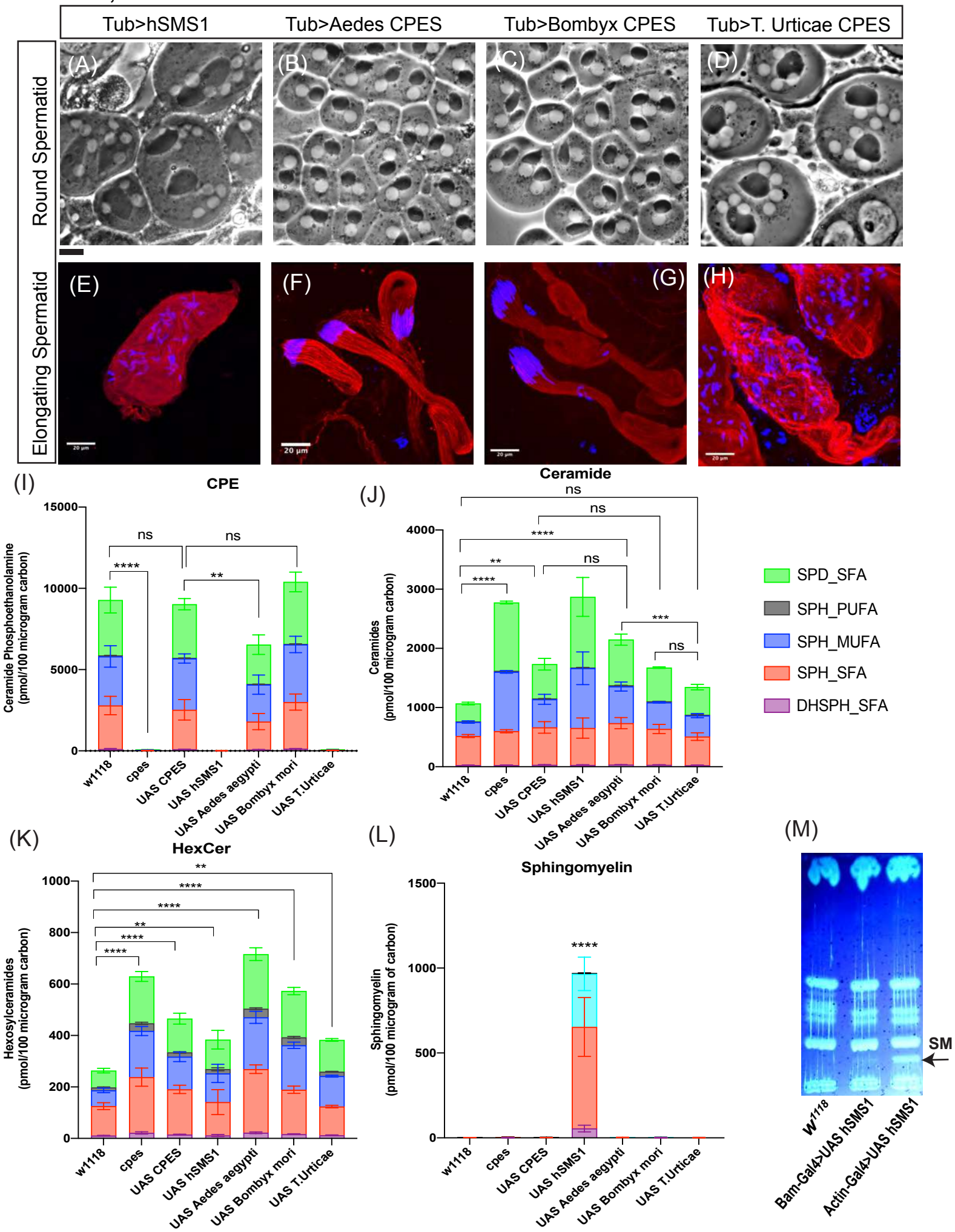

Figure 5
Kunduri et al., 2021

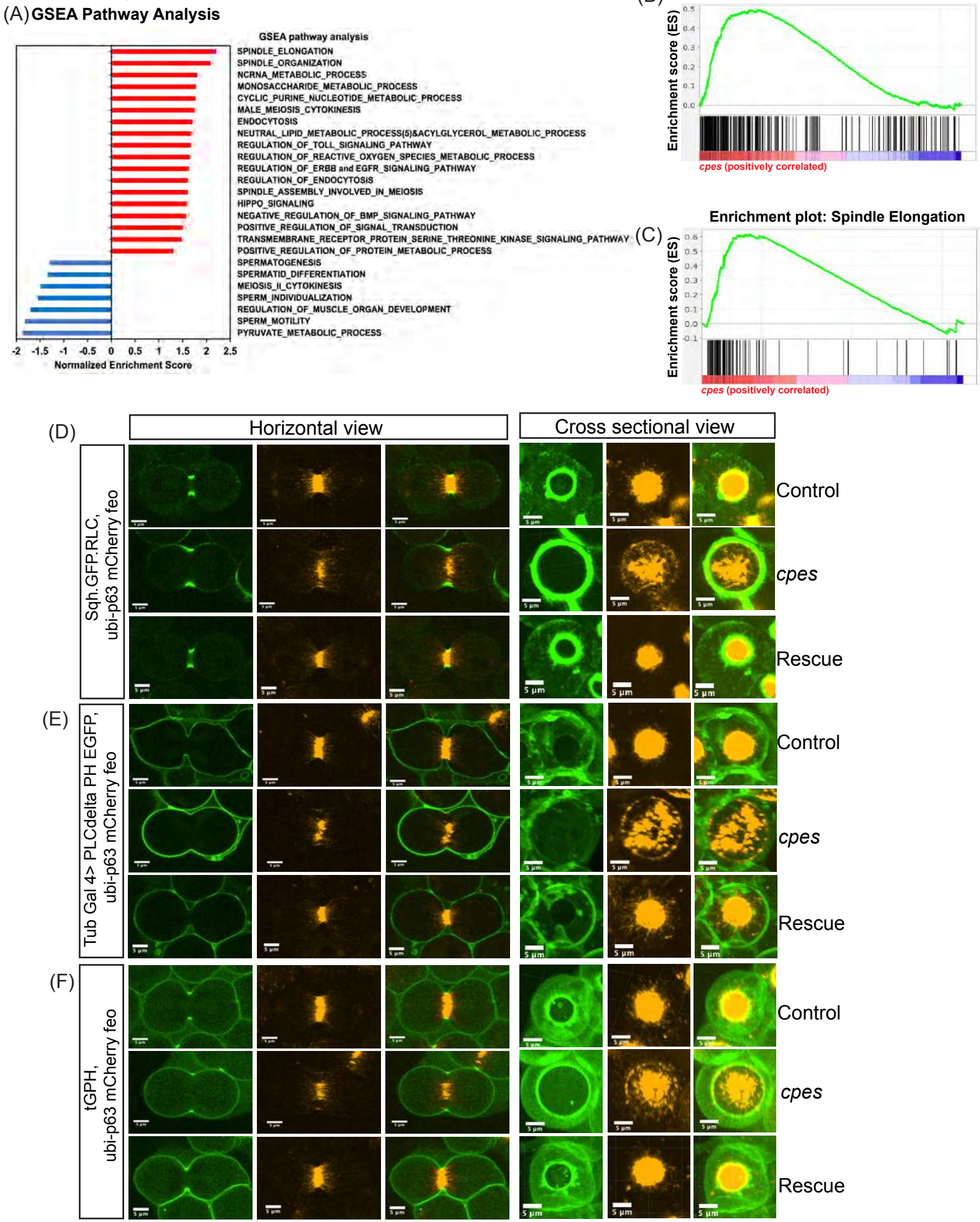

Figure 6
Kunduri et al., 2021

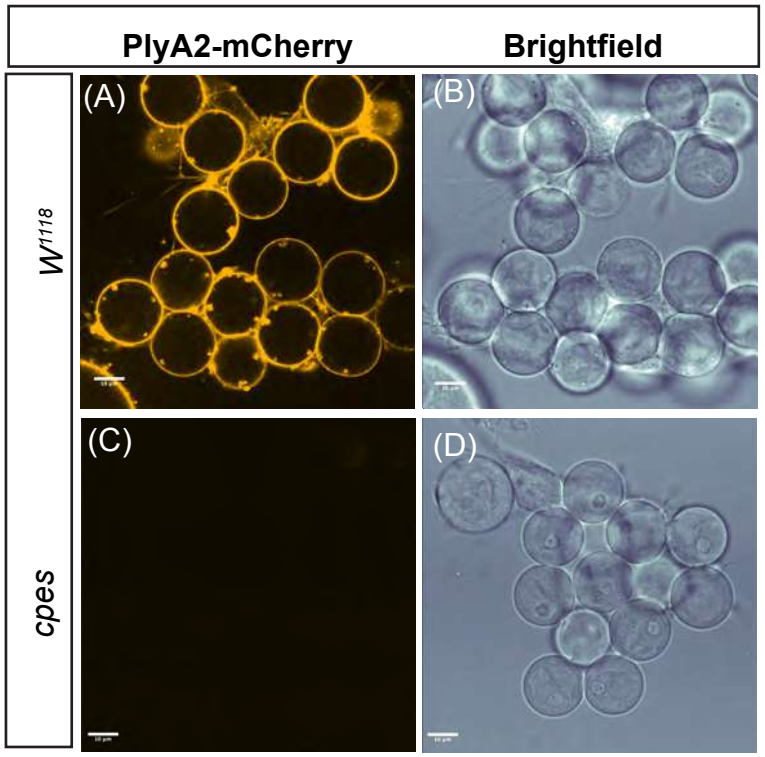

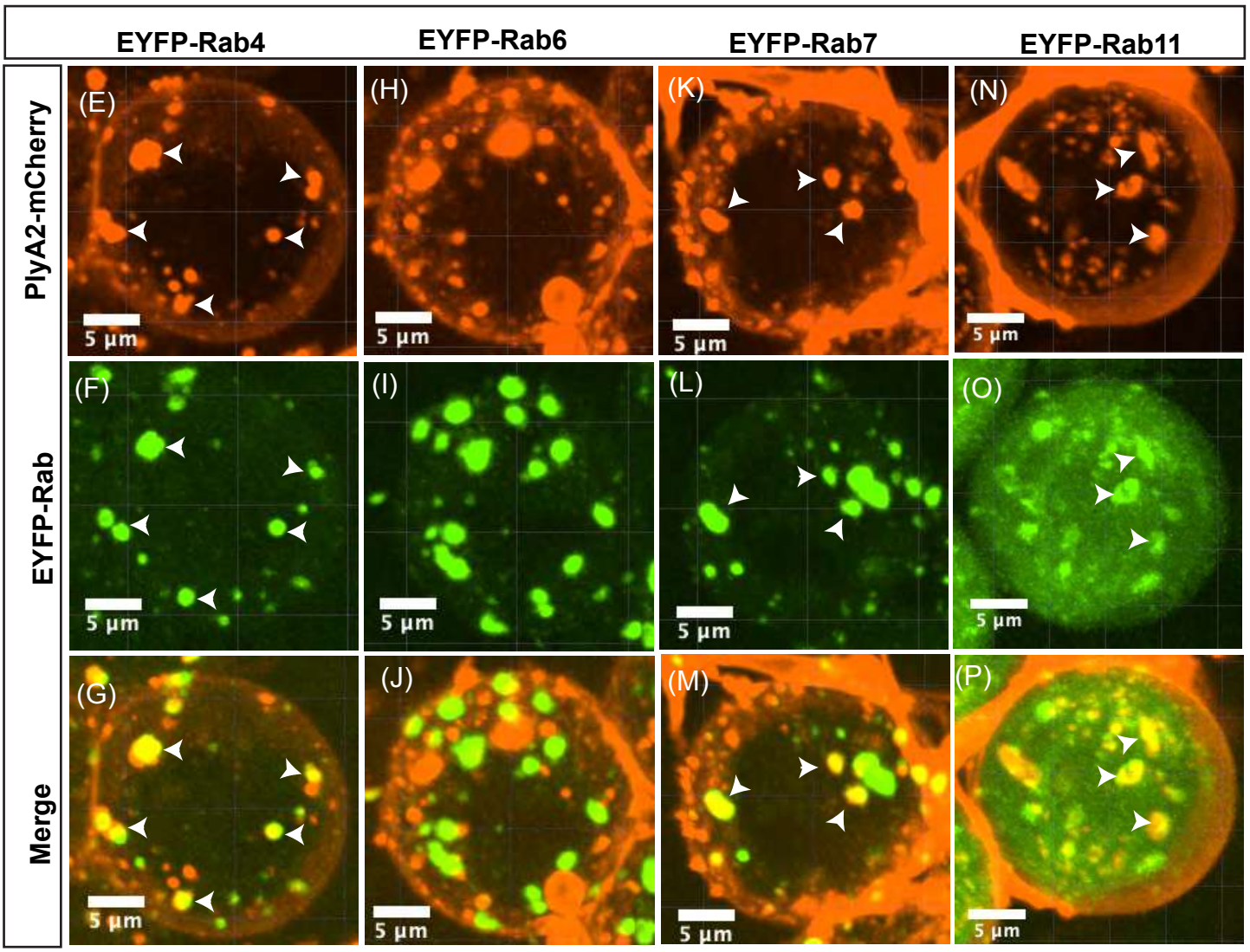
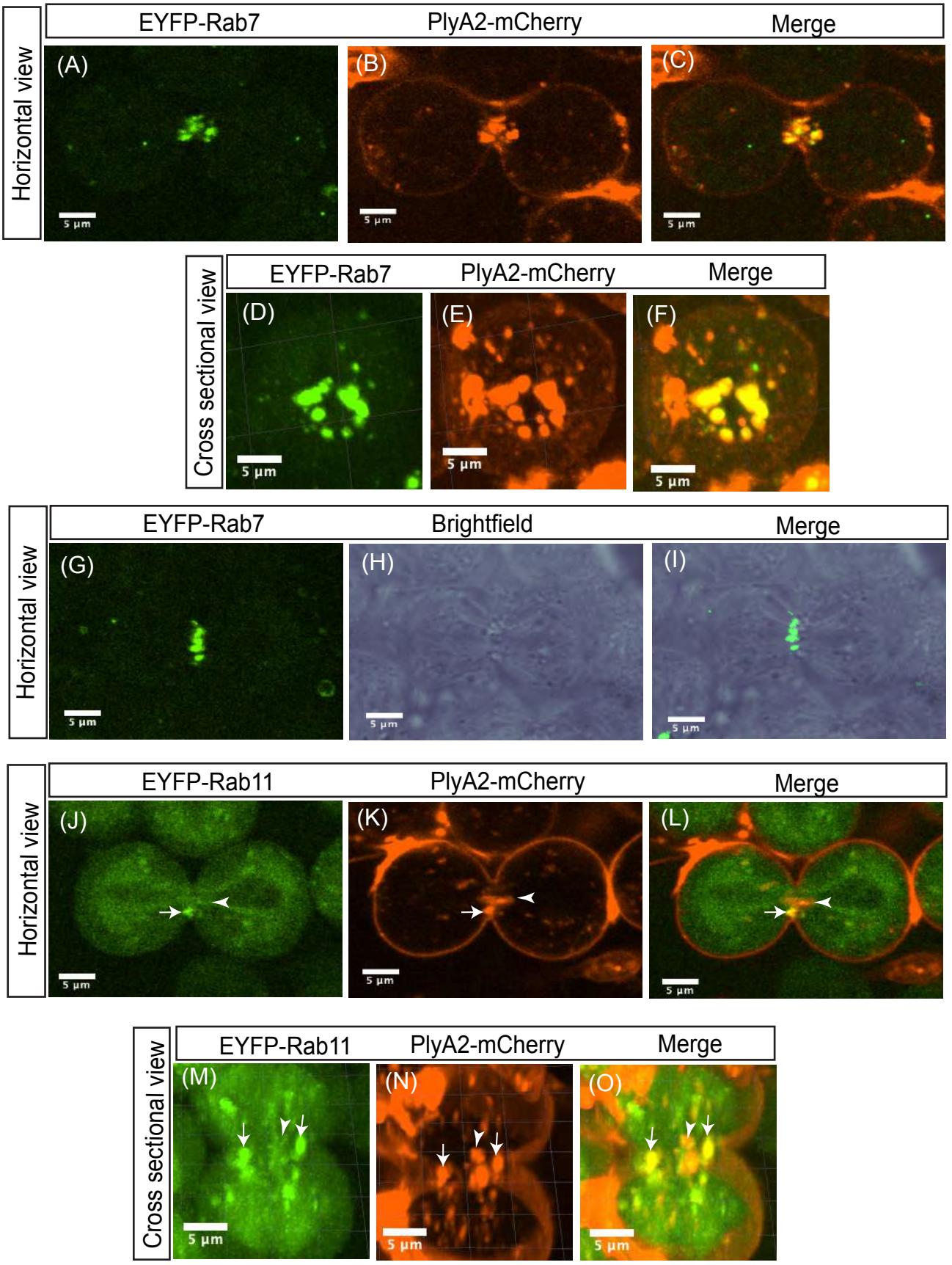
Figure 7
Kunduri et al., 2021